

Exclusive decays  $\chi_{cJ} \rightarrow K^*(892)K$  within the effective field theory  
framework

Nikolay Kivel

*Institut für Kernphysik, Johannes Gutenberg-Universität, D-55099, Mainz, Germany  
and*

*Petersburg Nuclear Physics Institute, Gatchina, 188300, St. Petersburg, Russia*

November 9, 2018

**Abstract**

We study hadronic decays  $\chi_{cJ} \rightarrow K^*(892)\bar{K}$  within the effective field theory framework. We consider the colour-singlet and colour-octet contributions and study their properties using (p)NRQCD effective theory. We show that infrared singularities in collinear integrals of the colour-singlet amplitudes can be absorbed into the renormalisation of the colour-octet matrix elements. The heavy quark spin symmetry allows us to establish a relation between the colour-octet matrix elements and to define the spin symmetry breaking corrections which are free from infrared singularities. We apply obtained results for a phenomenological description of the branching fractions.

# 1 Introduction

A study of heavy quark systems like charmonium and bottomonium has been one of the most interesting topic of particle physics for many years already. Many new interesting experimental results have been obtained by BABAR, BELLE, BESII and BESIII collaborations during last years. In particular, many new data about various exclusive decays have been collected and many new results are expected in the future. On the other side a theoretical description of various exclusive decay channels remains puzzling, see e.g. discussions in reviews [1, 2] and references therein. Often, underlying hadronic dynamics is very complicated and involves non-perturbative effects which are even difficult to include into a systematic theoretical description. One of such problematic contributions is the colour-octet mechanism [1, 3]. In inclusive processes such contributions are described as unknown long-distance matrix elements [4] but for exclusive decays a systematic description of such mechanism is still not well understood [1, 2]. At the same time such contributions can play an important role in the correct description of various exclusive amplitudes. In Ref. [8] it is suggested that the colour-octet configuration may play an important role for an understanding of the well known "ρπ-puzzle". Some attempts to build a framework for description of the colour-octet matrix elements can be found in Refs. [5–7]. In Ref. [31] it was shown that a correct description of colour-singlet amplitudes with infrared divergencies is related to the contribution of the colour-octet matrix elements.

In the present work we consider hadronic decays  $\chi_{cJ} \rightarrow K^* \bar{K}$  which are interesting because of specific properties of the corresponding amplitudes. The branching fractions of these decays have been measured by the BES collaboration [9, 10]. In Table 1 we collect experimental results from [11].

$\chi_{cJ} \rightarrow VP$	$K^*(892)^0 K^0 + c.c.$	$K^*(892)^+ K^- + c.c.$
$\chi_{c1}$	$10 \pm 4$	$15 \pm 7$
$\chi_{c2}$	$1.3 \pm 0.28$	$1.5 \pm 0.22$

Table 1: The branching fractions  $\chi_{cJ} \rightarrow K^* K$  in units of  $10^{-4}$ .

The amplitudes for these decays are closely related to the  $SU(3)$  flavour symmetry breaking effects in QCD and the experimental results for the decay rates indicate that such contributions are sufficiently large.

Another interesting point is that the decay amplitude of tensor state  $\chi_{c2}$  is suppressed according to the helicity selection rule [12–14]. Hence, this amplitude is sensitive to higher Fock components of mesonic wave functions. A sufficiently large value of the measured decay rates implies the strong violation of the helicity selection rule. In this respect this process could be similar to the decay  $J/\psi \rightarrow \rho\pi$  and probably have resembling underlying decay mechanism.

In Ref. [15] it is suggested that the amplitude for  $\chi_{c2} \rightarrow K^* K$  decay is dominated by a long distance decay mechanism which can be accounted through a model with intermediate mesonic loops. The obtained numerical estimate is about a factor two smaller then the experimental result. The second decay  $\chi_{c1} \rightarrow K^* K$  has not yet been discussed in the literature and we could not find any theoretical predictions for the corresponding decay width.

In our work we consider both decays within the effective field theory framework. We apply NRQCD [4, 16] and potential NRQCD (pNRQCD) [17–22] effective theories and soft collinear effective theory (SCET) [23–28] in order to describe decays of  $P$ -wave quarkonia into  $K^* \bar{K}$  mesons. An advantage of this framework is the opportunity to apply the heavy quark spin symmetry (HQSS) which allows one to constrain a contribution associated with the colour-octet mechanism. The latter can play an important role in the understanding of underlying mechanism of  $P$ -wave quarkonia decays [1, 5, 6].

The computation of colour-singlet contributions in the helicity suppressed decays involves different twist-2 and twist-3  $K$ -meson light-cone distribution amplitudes (DAs). However such contributions often have infrared (IR) divergencies that appear in the collinear convolution integrals. Then, a naive collinear factorisation is violated and colour-singlet mechanism can not be considered as only one possible contribution. Such situation often arises in the description of amplitudes involving the higher Fock components of hadronic wave functions. Rigorously speaking, a systematic description of such endpoint divergencies still remains challenging to theory.

Sometimes the structure of the IR divergencies allows one to conclude about the presence of a colour-octet matrix element. Such situation has been considered for amplitudes of  $B \rightarrow \chi_{c,J} \bar{K}$  decays in Ref. [31]. In this work it is shown that the endpoint singularities in the colour-singlet contribution can be absorbed into a colour-octet operator matrix element computed in the Coulomb limit.

In the present work we use the same idea, we will define and compute the relevant colour-octet matrix elements in the Coulomb limit. We also study the HQSS constraints for the colour-octet matrix elements of  $P$ -wave charmonia which are dictated by the structure of the effective Lagrangian where the interactions with the heavy quark spin are suppressed. The existence of a relation between the colour-octet matrix elements allows one to define a consistent IR subtraction scheme for a calculation of the spin symmetry breaking terms. Such technique, also known as physical subtraction scheme, is successfully used for the description of various amplitudes in  $B$ -decays, see *e.g.* Refs. [29,30].

Our paper is organised as follows: in Sec. 2 we set up the notation and define kinematics and amplitudes. In Sec. 3 we compute various colour-singlet contributions and study their properties. Sec. 4 is devoted to analysis of the colour-octet contributions in the Coulomb limit. The Sec. 5 is devoted to a phenomenological consideration. We discuss effects provided by the symmetry-breaking corrections and estimate a contribution of the colour-octet matrix elements. Then we conclude in Sec. 6.

## 2 Kinematics, notation and decay amplitudes

The decay amplitudes  $\chi_{c,J} \rightarrow \bar{K} + K^*$  are defined as

$$\langle \bar{K}(k) K^*(p); \text{out} | \text{in}; \chi_{c,J}(P) \rangle = i(2\pi)^4 \delta(P - p - k) \mathcal{M}_{\chi_{c,J} \rightarrow \bar{K} K^*}. \quad (1)$$

In what follows we use the frame where heavy meson is at rest and the  $z$ -axis is chosen along the momenta of outgoing particles

$$P = M(1, \vec{0}) = M\omega, \quad (2)$$

where  $M$  is charmonium mass and  $\omega$  denotes charmonium four-velocity. Any four-vector  $V$  which is orthogonal to velocity  $\omega$  is denoted with the subscript  $\perp$ :  $\omega \cdot V_\perp = 0$ .

The momenta of the outgoing mesons read

$$k = (k_0, 0, 0, k_z), \quad p = (p_0, 0, 0, p_z), \quad (3)$$

with (for simplicity, in the following we use  $m_{\bar{K}} \equiv m_P$  and  $m_{K^*} \equiv m_V$ )

$$k_0 = \frac{M^2 + m_P^2 - m_V^2}{2M}, \quad p_0 = \frac{M^2 - m_P^2 + m_V^2}{2M}, \quad (4)$$

$$k_z = -p_z = \frac{1}{2M} \left[ \left( M^2 - (m_V - m_P)^2 \right) \left( M^2 - (m_V + m_P)^2 \right) \right]^{1/2}. \quad (5)$$

Assuming that the heavy quark mass is sufficiently large  $m_c \gg \Lambda_{QCD}$  one obtains

$$k \simeq m_c(1, 0, 0, 1) = 2m_c \frac{\bar{n}}{2}, \quad p \simeq m_c(1, 0, 0, -1) = 2m_c \frac{n}{2}, \quad (6)$$

where we introduced auxiliary light-cone vectors  $n$  and  $\bar{n}$  with  $(n\bar{n}) = 2$ . Any four-vector  $V^\mu$  can be decomposed as

$$V^\mu = (V \cdot n) \frac{\bar{n}^\mu}{2} + (V \cdot \bar{n}) \frac{n^\mu}{2} + V_\perp^\mu, \quad (7)$$

where  $V_\perp$  denotes the components which are transverse to the light-like vectors:  $(V_\perp \cdot n) = (V_\perp \cdot \bar{n}) = 0$ . In particular, in the rest frame

$$\omega = \frac{1}{2}(n + \bar{n}), \quad \omega^2 = 1. \quad (8)$$

In the following we also use short notations

$$g_\perp^{\mu\nu} = g^{\mu\nu} - \frac{1}{2}(n^\mu \bar{n}^\nu + n^\nu \bar{n}^\mu), \quad i\varepsilon_\perp^{\mu\nu} = \frac{1}{2}i\varepsilon_{\mu\nu\alpha\beta} n^\alpha \bar{n}^\beta, \quad (9)$$

with  $\varepsilon_{0123} = 1$ . The decay amplitudes can be parametrised as

$$\mathcal{M}_{\chi_{c1} \rightarrow \bar{K}K^*} = (\epsilon_\chi \cdot k) (e_V^* \cdot k) \frac{m_V}{M^2} \mathcal{A}_1^\parallel + (\epsilon_{\chi\perp} \cdot e_{V\perp}^*) \frac{(kP)}{M} \mathcal{A}_1^\perp, \quad (10)$$

$$\mathcal{M}_{\chi_{c2} \rightarrow \bar{K}K^*} = \epsilon_\chi^{\mu\nu} k_\nu i \varepsilon_{\mu\alpha\beta\rho} (e_V^*)^\alpha \frac{k^\beta p^\rho}{(kp)} \mathcal{A}_2^\perp, \quad (11)$$

where  $\epsilon_\chi$  and  $e_V^*$  denote polarisation vectors of the charmonium states and vector meson, respectively. The polarisation vectors satisfy

$$\sum_\lambda (\epsilon_\chi^{(\lambda)})_\mu (\epsilon_\chi^{(\lambda)})_\nu^* = -g_{\mu\nu} + P_\mu P_\nu / M^2, \quad (12)$$

$$\sum_\lambda (\epsilon_\chi^{(\lambda)})_{\mu\nu} (\epsilon_\chi^{(\lambda)})_{\rho\sigma}^* = \frac{1}{2} G_{\mu\rho} G_{\nu\sigma} + \frac{1}{2} G_{\mu\sigma} G_{\nu\rho} - \frac{1}{3} G_{\mu\nu} G_{\rho\sigma}, \quad (13)$$

where  $G_{\mu\nu} = g_{\mu\nu} - P_\mu P_\nu / M^2$ , the normalization is such that  $(\epsilon_\chi^{(\lambda)})_{\mu\nu} (\epsilon_\chi^{(\lambda')})_{\mu\nu}^* = \delta_{\lambda\lambda'}$ ,  $(\epsilon_\chi^{(\lambda)})_\mu (\epsilon_\chi^{(\lambda')})_\mu^* = \delta_{\lambda\lambda'}$  and similar for the  $K^*$  vector meson.

The kinematical factors in Eqs.(10) and (11) are chosen in order to have dimensionless amplitudes  $\mathcal{A}_i$ . One can easily see that amplitude  $\mathcal{A}_1^\parallel$  describes decay of the longitudinally polarised  $\chi_{c1}$  while the amplitudes  $\mathcal{A}_{1,2}^\perp$  correspond to transversely polarised  $\chi_{c1,2}$ . The expressions for decay widths read

$$\Gamma[\chi_{c1} \rightarrow \bar{K}K^*] = \frac{|\vec{k}|^2}{8\pi} \frac{k_0^2}{3M^2} \left( |\mathcal{A}_1^\perp|^2 + \frac{1}{2} \frac{(pk)^2}{M^4} |\mathcal{A}_1^\parallel|^2 \right), \quad (14)$$

$$\Gamma[\chi_{c2} \rightarrow \bar{K}K^*] = \frac{|\vec{k}|^2}{8\pi} \frac{k_0^2}{5M^2} |\mathcal{A}_2^\perp|^2 \left( 1 - \frac{m_P^2}{k_0^2} \right) \left( 1 - \frac{m_P^2 m_V^2}{(kp)^2} \right). \quad (15)$$

### 3 Colour-singlet contributions

#### 3.1 Colour-singlet contribution to amplitude $\mathcal{A}_1^\parallel$

A computation of the colour-singlet contribution is quite standard, corresponding contribution is described by the diagrams in Fig.1. The heavy quark and antiquark annihilate at short distance of order  $1/m_c$  into the two highly virtual gluons which further create light quark-antiquark pairs forming the final mesons. An average size of the charmonium is of order  $1/m_c v$  where  $v$  is the heavy quark velocity in the rest frame. Since  $m_c v \ll m_c$  the colour-singlet decay amplitude is proportional to the heavy meson wave function at the origin. Corresponding contribution can be described by a matrix element of the appropriate colour-singlet operator in NRQCD framework.

Transitions of the light quarks into final mesons also involve non-perturbative QCD interactions associated with the typical hadronic scale  $\Lambda \ll m_c$ . In charmonium rest frame energies of the outgoing mesons are large, of order  $m_c$  and corresponding non-perturbative contributions are described by the light-cone matrix elements which are related to the light-cone wave functions at zero transverse separation, the so-called light-cone distribution amplitudes (DAs). Detailed description of these quantities is given in Appendix A.

All matrix elements arising in description of the amplitudes can be estimated according to the power counting with respect to small parameters: velocity  $v$  and ratio  $\Lambda/m_c$ . At the leading-order we only have contribution to amplitude  $\mathcal{A}_1^\parallel$ . In this case the soft overlaps with the *in* and *out* mesonic states are described by the leading-order NRQCD matrix element and by the leading twist DAs  $\phi_{2V}^\parallel$  and  $\phi_{2P}$  where the subscripts  $V$  and  $P$  denote the vector and pseudoscalar mesons. In the following we always assume  $V \equiv K^*$  and  $P \equiv \bar{K}$ . The transverse amplitudes  $\mathcal{A}_{1,2}^\perp$  are suppressed by the power of  $\Lambda/m_c$  due to the helicity conservation in the hard subprocess. As a result they depend on the twist-3 DAs and this provides suppression by extra power of the small ratio  $\Lambda/m_c$ .

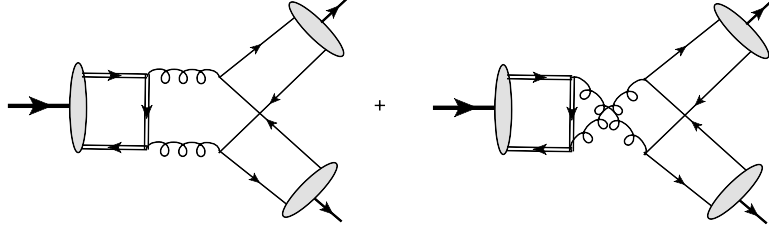


Figure 1: The QCD diagrams describing the colour-singlet mechanism of  $\chi_{cJ} \rightarrow VP$  decays. The blobs denote various non-perturbative matrix elements.

The computation of the diagrams in Fig.1 with the appropriate operator projections gives the following result

$$\mathcal{A}_1^\parallel = -\frac{f_V^\parallel f_P}{m_c^2} i \langle \mathcal{O}({}^3P_1) \rangle \left( \frac{\pi \alpha_s(\mu^2)}{N_c} \right)^2 C_F J_c^\parallel(\mu), \quad (16)$$

with the collinear convolution integral ( $1-x \equiv \bar{x}$ )

$$J_c^\parallel(\mu) = \int_0^1 dx \frac{\phi_{2V}^\parallel(x, \mu)}{x\bar{x}} \int_0^1 dy \frac{\phi_{2P}(y, \mu)}{y\bar{y}} \frac{y-x}{xy + \bar{x}\bar{y}}. \quad (17)$$

We also use the standard notation  $C_F = (N_c^2 - 1)/(2N_c)$  with  $N_c = 3$ . The factorisation scale  $\mu$  is of order of the hard scale  $m_c$ . The definitions of the non-perturbative constants  $f_V^\parallel$ ,  $f_P$  and  $\langle \mathcal{O}({}^3P_1) \rangle$  can be found in Appendix A. According to NRQCD counting rules  $\langle \mathcal{O}({}^3P_1) \rangle \sim v^4$  and ratio  $f_V^\parallel f_P/m_c^2 \sim (\Lambda/m_c)^2$ . Hence from Eq.(16) one obtains

$$\mathcal{A}_1^\parallel \sim v^4 \left( \frac{\Lambda}{m_c} \right)^2. \quad (18)$$

From Eq.(17) one can see that the hard kernel is antisymmetric with respect to interchange  $\{x, y\} \rightarrow \{\bar{x}, \bar{y}\}$  and therefore the collinear integral is proportional to antisymmetric combinations  $\phi_{2V}^\parallel(x) - \phi_{2V}^\parallel(\bar{x})$  or  $\phi_{2P}(y) - \phi_{2P}(\bar{y})$  in Eq.(17). Such combinations do not vanish for  $K$ -meson DAs due to the  $SU(3)$  breaking. Using models for the distribution amplitudes as in Eqs.(106) and (114) one obtains

$$J_c^\parallel = \frac{27}{2} (\pi^2 - 4) \left( b_1(\mu) - a_{1V}^\parallel(\mu) \right) + \frac{27}{2} (6\pi^2 - 44) \left( b_1(\mu) a_{2V}^\parallel(\mu) - a_{1V}^\parallel(\mu) b_2(\mu) \right), \quad (19)$$

where  $b_{iP}$  and  $a_{iV}^\parallel$  are parameters of the DAs, see Appendix A. The moments  $a_{1V}^\parallel$  and  $b_1$  vanish in the exact  $SU(3)$  limit which explicitly demonstrates the dependence of the integral  $J_c^\parallel$  from the flavour symmetry violation.

Consider the branching fraction of  $\chi_{c1}$  state assuming that the transverse amplitude  $\mathcal{A}_1^\perp$  is small and can be neglected. In order to obtain numerical estimate we take  $c$ -quark mass  $m_c = 1.5$  GeV,  $\Lambda_{QCD}^{(4)} = 310$  MeV (this gives  $\alpha_s(2m_c^2) = 0.29$ ), the total width  $\Gamma[\chi_{c1}] = 0.84$  MeV. Numerical values of other parameters are given in Appendix A. Varying the factorisation scale  $\mu^2$  between  $m_c^2$  and  $4m_c^2$  we obtain

$$\text{Br}[\chi_{c1} \rightarrow \bar{K}^0 K^* (892)^0 + c.c.] = (0.02 - 0.06) \times 10^{-3}. \quad (20)$$

We see that this value is about two orders of magnitude smaller than the experimental branching fraction, see Table 1. This result allows one to conclude that the dominant numerical contribution is most probably provided by the amplitude  $\mathcal{A}_1^\perp$ . This conclusion does also agree with sufficiently large value of the branching ratio for the  $\chi_{c2}$  decay.

### 3.2 Colour-singlet contributions to amplitudes $\mathcal{A}_{1,2}^\perp$

Calculation of the colour-singlet contributions to amplitudes  $\mathcal{A}_{1,2}^\perp$  is more complicated because there are two different configurations: twist-2 and twist-3 projections for  $\bar{K}$  and  $\bar{K}^*$  states, respectively ( $P_2V_3$

contribution) and vice versa ( $P_3V_2$  contribution). In general, the twist-3 projections include contributions from two-particle and three-particle operators. The matrix elements of three-particle operators are given by the quark-gluon operators which are often referred as genuine twist-3 contributions. Using QCD equation of motions the matrix elements of two-particle twist-3 operators can be rewritten in terms of twist-2 and genuine twist-3 quark-gluon DAs, see *e.g.* Ref. [42]. In this work we neglect the contributions of three-particle quark-gluon operators in order to simplify our analysis. Discarding of the genuine twist-3 contributions is not a rigorous approximation but in a phenomenological calculations it is often considered as a reliable estimate of higher twist effects.<sup>1</sup> Hence we need to consider only the matrix elements of two-particle twist-3 operators neglecting the quark-gluon DAs. Such approximation is also known as Wandzura-Wilczek (WW) approximation. In this case one has to compute the same diagrams as in Fig.1 but keeping only twist-2 DAs in the twist-3 projections for two-particle collinear matrix elements. In order to make our notations simpler we do not introduce any special notation for twist-3 DAs in the WW approximation assuming that this is clear from the context.

The calculation is quite standard and we do not discuss here the technical details. The following results has been obtained( remind that  $V \equiv K^*$ ,  $P \equiv \bar{K}$ )

$$\mathcal{A}_{Jc}^{\perp(0)} = \frac{i \langle \mathcal{O}^3 P_J \rangle}{m_c^3} \left( \frac{\pi \alpha_s}{N_c} \right)^2 C_F 2^{J/2} \left\{ \frac{f_P f_V^{\parallel} m_V}{m_c^3} J_c^{(J)} [P_2 V_3] + \frac{f_P \mu_P f_V^{\perp}}{m_c^3} J_c^{(J)} [P_3 V_2] \right\}, \quad (21)$$

where the subscript “c” is introduced in order to stress the collinear operator structure for the final mesonic state. The collinear convolution integrals  $J_c^{(J)}$  read

$$J_c^{(J)} [P_2 V_3] = \frac{1}{8} \int_0^1 dy \frac{\bar{\phi}_{2P}(y)}{y\bar{y}} \int_0^1 \frac{dx}{x\bar{x}} \left\{ C_+^{(J)}(x, y) \int_x^1 du \frac{\Delta\Omega(u)}{u} + C_-^{(J)}(x, y) \int_0^x du \frac{\Delta\Omega(u)}{\bar{u}} \right\} \\ + \frac{1}{8} \int_0^1 dy \frac{\Delta\phi_{2P}(y)}{y\bar{y}} \int_0^1 \frac{dx}{x\bar{x}} \left\{ C_+^{(J)}(x, y) \int_x^1 du \frac{\bar{\Omega}(u)}{u} + C_-^{(J)}(x, y) \int_0^x du \frac{\bar{\Omega}(u)}{\bar{u}} \right\}. \quad (22)$$

Here we used convenient notation for the symmetric and antisymmetric combinations

$$\bar{\phi}(x) = \frac{1}{2}(\phi(x) + \phi(\bar{x})), \quad \Delta\phi(x) = \frac{1}{2}(\phi(x) - \phi(\bar{x})), \quad \bar{x} \equiv 1 - x. \quad (23)$$

The hard kernels in Eq.(22) read

$$C_-^{(1)}(x, y) = \frac{2\bar{x}}{(xy + \bar{x}\bar{y})} - \frac{\bar{x}(x + \bar{y})}{(xy + \bar{x}\bar{y})^2}, \quad C_+^{(1)}(x, y) = \frac{2\bar{x} - 1}{xy + \bar{x}\bar{y}} + \frac{\bar{x}(y - \bar{x})}{(xy + \bar{x}\bar{y})^2}. \quad (24)$$

$$C_-^{(2)}(x, y) = \frac{\bar{x}(x + \bar{y})}{(xy + \bar{x}\bar{y})^2}, \quad C_+^{(2)}(x, y) = -\frac{x(\bar{x} + y)}{(xy + \bar{x}\bar{y})^2}. \quad (25)$$

The function  $\Omega(u)$  is defined in Eq.(117) in Appendix A .

For the convolution integral describing  $P_3V_2$  projection can be written as

$$J_c^{(J)} [P_3 V_2] = \frac{(-1)}{48} \int_0^1 dx \frac{\bar{\phi}_{2V}^{\perp}(x)}{x\bar{x}} \int_0^1 dy \frac{\tilde{C}_\sigma^{(J)}(x, y) \Delta\phi_{3P}^{\sigma'}(y) + C_p^{(J)}(x, y) \Delta\phi_{3P}^p(y) + C_\sigma^{(J)}(x, y) \Delta\phi_{3P}^\sigma(y)}{y\bar{y}(xy + \bar{x}\bar{y})^2} \\ + \frac{(-1)}{48} \int_0^1 dx \frac{\Delta\phi_{2V}^{\perp}(x)}{x\bar{x}} \int_0^1 dy \frac{\tilde{C}_\sigma^{(J)}(x, y) \bar{\phi}_{3P}^{\sigma'}(y) + C_p^{(J)}(x, y) \bar{\phi}_{3P}^p(y) + C_\sigma^{(J)}(x, y) \bar{\phi}_{3P}^\sigma(y)}{y\bar{y}(xy + \bar{x}\bar{y})^2}, \quad (26)$$

where

$$\tilde{C}_\sigma^{(J=1)} = (y - \bar{y})(y - \bar{x}), \quad \tilde{C}_\sigma^{(J=2)} = (1 + y\bar{y} - x\bar{x} - (x - y)^2), \quad (27)$$

$$C_p^{(J=1)} = 6(\bar{x} - y + 2(y - \bar{y})(xy + \bar{x}\bar{y})), \quad C_p^{(J=2)} = 6(y - \bar{x}), \quad (28)$$

$$C_\sigma^{(J=1)} = 4(\bar{x} - y), \quad C_\sigma^{(J=2)} = 4(y - \bar{x}). \quad (29)$$

<sup>1</sup>Let us also add that such approximation does not contradict to the Lorentz and gauge symmetries in QCD

The explicit expressions for DAs  $\phi_{3P}^{\sigma,P}$  and  $\phi_{2V}^\perp$  are given in Eqs.(107),(108) and (114), the prime denotes derivative with respect to collinear fraction:  $\phi'(x) \equiv d/dx\phi(x)$ . From Eq.(21) one can easily conclude that the transverse amplitudes behave as

$$\mathcal{A}_{J_c}^{\perp(0)} \sim v^4 \left( \frac{\Lambda}{m_c} \right)^3, \quad (30)$$

and these contributions are suppressed compared to  $\mathcal{A}_1^\parallel$ . On the other side, amplitudes  $\mathcal{A}_J^\perp[P_3V_2]$  include the so-called chiral enhanced coefficient  $\mu_P$ , see Eq.(105), which is numerically large. Taking into account the real value of the  $c$ -quark mass one finds that  $\mu_P/m_c \sim 1$  and therefore such corrections can provide a large effect.

The convolution integrals  $J_c^{(J)}$  have logarithmic IR-divergencies associated with the endpoint regions  $y \rightarrow 0, x \rightarrow 1$  and  $y \rightarrow 1, x \rightarrow 0$ . These are the so-called endpoint divergencies which indicate about the logarithmic overlap with the ultrasoft domain. In order to single out these divergencies one needs to perform an expansion of the integrands in the corresponding regions.

Consider, for instance, the first integral in Eq.(26) which has the following integrand

$$F(x, y) = \frac{\bar{\phi}_{2V}^\perp(x)}{x\bar{x}} \frac{\tilde{C}_\sigma^{(J)}(x, y) \Delta\phi_{3P}^{\sigma'}(y) + \dots}{y\bar{y}(xy + \bar{x}\bar{y})^2}, \quad (31)$$

here the dots denote the other terms in the numerator of Eq.(26). Using models of DAs from Appendix A one easily finds the following useful relations

$$\lim_{x \rightarrow 1} \bar{\phi}_{2V}^\perp(x) = -\bar{x}\bar{\phi}_{2V}^{\perp'}(1), \quad \lim_{x \rightarrow 0} \bar{\phi}_{2V}^\perp(x) = x\bar{\phi}_{2V}^{\perp'}(0), \quad (32)$$

$$\lim_{y \rightarrow 0} \Delta\phi_{3P}^p(y) = \rho_-^K \frac{3}{2} (\alpha + \beta \ln y) \equiv \Delta\phi_{3P}^p(y \sim 0), \quad \alpha = 1 + 21b_2, \beta = 1 + 6b_2, \quad (33)$$

$$\lim_{y \rightarrow 0} \Delta\phi_{3P}^{\sigma'}(y) = 6\Delta\phi_{3P}^p(y \sim 0), \quad \lim_{y \rightarrow 1} \Delta\phi_{3P}^{\sigma'}(y) = -6\Delta\phi_{3P}^p(y \sim 1), \quad (34)$$

$$\lim_{y \rightarrow 1} \Delta\phi_{3P}^p(y) = -\rho_-^K \frac{3}{2} (\alpha + \beta \ln \bar{y}) \equiv \Delta\phi_{3P}^p(y \sim 1). \quad (35)$$

Hence the expansion of integrand in Eq.(31) in the endpoint regions gives

$$F(x, y)|_{y \sim \bar{x} \rightarrow 0} = (-1)^{J+1} 4\bar{\phi}_{2V}^{\perp'}(1) \frac{6\Delta\phi_{3P}^p(y \sim 0)}{(y + \bar{x})^2} \equiv F(x \sim 1, y \sim 0), \quad (36)$$

$$F(x, y)|_{x \sim \bar{y} \rightarrow 0} = (-1)^{J+1} 4\bar{\phi}_{2V}^{\perp'}(0) \frac{6\Delta\phi_{3P}^p(y \sim 1)}{(x + \bar{y})^2} \equiv F(x \sim 0, y \sim 1). \quad (37)$$

The corresponding convolution integral in Eq.(26) can be rewritten as a sum of the regular and singular terms

$$\int_0^1 dx \int_0^1 dy F(x, y) = I_{\text{reg}} + I_{\text{sing}}, \quad (38)$$

with

$$\begin{aligned} I_{\text{reg}} &= \int_0^1 dx \int_0^1 dy \{F(x, y) - F(x \sim 1, y \sim 0) - F(x \sim 0, y \sim 1)\}, \\ I_{\text{sing}} &= \int_0^1 dx \int_0^1 dy \{F(x \sim 1, y \sim 0) + F(x \sim 0, y \sim 1)\}, \end{aligned} \quad (39)$$

where only the integrals  $I_{\text{sing}}$  are IR-divergent. In order to regularise them we apply analytic regularisation modifying the heavy quark propagator. We imply that the regularisation is introduced *after*

differentiation with respect to relative momentum  $\Delta_\top$  ( as required by projection on quarkonium  $P$ -wave state)

$$\frac{1}{[m_c^2(xy + \bar{x}\bar{y})]^n} \rightarrow \frac{\nu^{2\varepsilon}}{[m_c^2(xy + \bar{x}\bar{y})]^{n+\varepsilon}}, \quad (40)$$

where  $\nu$  is the renormalisation scale. With such regulator one obtains

$$I_{\text{sing}} = (-1)^{J+1} 4\bar{\phi}_{2V}^{\perp'}(1) t^\varepsilon \int_0^1 dx \int_0^1 dy \left\{ \frac{6\Delta\phi_{3P}^p(y \sim 0)}{(y + \bar{x})^{2+\varepsilon}} - \frac{6\Delta\phi_{3P}^p(y \sim 1)}{(\bar{y} + x)^{2+\varepsilon}} \right\}, \quad (41)$$

where  $t \equiv \nu^2/m_c^2$  and we used that  $\bar{\phi}_{2V}^{\perp'}(1) = -\bar{\phi}_{2V}^{\perp'}(0)$ . A simple but lengthy calculation yields

$$I_{\text{sing}} = (-1)^{J+1} \bar{\phi}_{2V}^{\perp'}(1) 72\rho_-^K \times \left( -\frac{\beta}{\varepsilon^2} - \beta \frac{\ln t}{\varepsilon} - (\alpha - \beta) \frac{1}{\varepsilon} - \beta \frac{1}{2} \ln^2 t - (\alpha - \beta) \ln t + \beta \frac{\pi^2}{12} - (\alpha - \beta) - \alpha \ln 2 \right). \quad (42)$$

The double IR-pole in  $1/\varepsilon$  arises due to the presence of logarithms  $\ln y$  and  $\ln \bar{y}$  in Eqs.(33) and (35). Hence for the first integral from Eq.(26) we obtain

$$J_{c1}^{(J)}[P_3V_2] = -\frac{1}{48} \int_0^1 dx \int_0^1 dy F(x, y) \\ = (-1)^J \bar{\phi}_{2V}^{\perp'}(1) \frac{3}{2} \rho_-^K \left( -\frac{\beta}{\varepsilon^2} - \beta \frac{\ln t}{\varepsilon} - (\alpha - \beta) \frac{1}{\varepsilon} - \beta \frac{1}{2} \ln^2 t - (\alpha - \beta) \ln t \right) + \dots, \quad (43)$$

where dots denote the remnant finite terms. The same technique can also be used for other convolution integrals in Eqs.(22) and (26). These integrals also have IR-divergencies which produce double and single poles in  $1/\varepsilon$ .

A study of structure of the divergent integrals can be helpful in order to identify an operator which can be associated with the IR-divergencies. The intermediate gluons in the diagrams in Fig.1 have momenta  $yk + \bar{x}p$  and  $\bar{y}k + xp$ . Hence in the regions  $y \sim \bar{x} \rightarrow 0$  or  $x \sim \bar{y} \rightarrow 0$  one of the gluons has a very small momentum while the second gluon still has the hard momentum. It is natural to assume that gluon with the small momentum is ultrasoft, i.e. in the endpoint regions we have  $yk + \bar{x}p \sim m_c v^2$  or  $\bar{y}k + xp \sim m_c v^2$  which is equivalent to  $y \sim \bar{x} \sim v^2$  or  $x \sim \bar{y} \sim v^2$ . The interactions of such ultrasoft gluons with a soft heavy quark  $p_Q \sim m_c v$  does not change its virtuality. Therefore in the endpoint domain the momentum of the virtual heavy quark in diagrams in Fig.1 is soft. The corresponding propagators yield combinations  $(y + \bar{x})^{-2}$  or  $(x + \bar{y})^{-2}$  in the kernels of Eqs.(36) and (37) and these terms produce the IR-divergencies in the convolution integrals.

Therefore in the endpoint regions the hard subprocess is different and can be described by the hard annihilation of heavy quark-antiquark pair into the light quark-antiquark pair with light-like momenta:  $c\bar{c} \rightarrow g^* \rightarrow q + \bar{q}$  or  $c\bar{c} \rightarrow g^* \rightarrow s + \bar{s}$ . Since the annihilation produces only one hard gluon the corresponding heavy quark-antiquark pair must be in the colour-octet state. This allows one to conclude that a colour-octet matrix element must be added into the consideration in order to explain IR-divergencies of the colour-singlet contribution. It is obvious that such octet contribution must have the same behaviour in  $v$  as the singlet one in Eq.(30).

The mixing of singlet and octet mechanisms in exclusive decays within the effective theory framework has already been studied in Ref. [31]. In present case the situation is similar but a bit more complicated from the technical point of view because of double IR-poles, see Eq.(42). In the realistic world the colour-octet contribution is non-perturbative because of relatively small charm mass. However in the next section we consider corresponding matrix element in the Coulomb limit which allows one to perform calculations within the pNRQCD framework. Such consideration allows one explicitly to verify the correspondence of divergencies between the colour-singlet and colour-octet terms. If IR-poles in colour-singlet matrix element are reproduced as UV-poles of the colour-octet contribution then the IR-poles can be absorbed into the renormalisation of the colour-octet matrix element.

Let us consider some qualitative arguments based on the spin symmetry of the effective field theory in the limit  $m_c \rightarrow \infty$ . It is well known that the HQSS provides approximate relations between matrix



elements for the various states of a given radial and orbital excitation of heavy quarkonium. The violation of the heavy-quark spin symmetry related with the higher order terms in effective Lagrangian suppressed by powers of  $v$ . The example of such relations for the wave functions are well known [4] and used in Eqs.(98-100). Despite the colour-octet operators are more complicated the effective heavy quark Lagrangian is the same and this also can provide an approximate relations between the various octet matrix elements.

The relevant for our case hard subprocess is  $c\bar{c} \rightarrow g^* \rightarrow q + \bar{q}$  and hard factorisation yields the four-quark operators

$$C_h \bar{q} \gamma_\sigma t^a q \chi_\omega^\dagger \gamma_\tau^\sigma t^a \psi_\omega, \quad (44)$$

where  $C_h$  is the hard coefficient function,  $t^a$  denotes the SU(3) color matrices,  $q$  denotes the light quark field,  $\psi_\omega$  and  $\chi_\omega^\dagger$  denote quark and antiquark four-component spinors in the NRQCD, see more details in Appendix A. Then the colour-octet amplitude is schematically given by the matrix element

$$\mathcal{A}_J^{\perp(8)} = C_h \langle K^* \bar{K} | \bar{q} \gamma_\sigma t^a q \chi_\omega^\dagger \gamma_\tau^\sigma t^a \psi_\omega | \chi_J(\omega) \rangle. \quad (45)$$

According to NRQCD counting rules, the bilinear heavy quark operator is of order  $v^3$ . In order to get a contribution of order  $v^4$  which can mix with the colour-singlet contribution in (30) one needs an interaction of order  $v$ . In pNRQCD Lagrangian such interaction is only described by chromoelectric dipole vertex  $\sim \psi_\omega^\dagger(x) \vec{x} \cdot \vec{E}(t) \psi_\omega(x)$  which is not sensitive to the heavy quark spin. Therefore we can conclude that HQSS can also relate the matrix elements (45) with the different  $J = 1, 2$ . In Sec. 4 it will be shown that in the weak coupling limit  $|p_{us}| \gg \Lambda$  this yields

$$\mathcal{A}_{J=1}^{\perp(8)} = -\frac{1}{\sqrt{2}} \mathcal{A}_{J=2}^{\perp(8)}. \quad (46)$$

up to higher order corrections in small velocity  $v$ . The next important step is the assumption that at given order the total result for the physical amplitude is only given by the sum of the singlet and octet amplitudes. Then the various factorisation scales which appears in these contributions must cancel in the sum

$$\mathcal{A}_J^\perp = \mathcal{A}_J^{\perp(0)} + \mathcal{A}_J^{\perp(8)}. \quad (47)$$

Such compensation in some sense is equivalent to a cancellation of singularities in the *rhs* of Eq. (47), therefore this implies that divergent integrals in the colour-singlet amplitudes must also satisfy to relation (46). Then the hard contributions which violate spin-symmetry relations must be well defined, i.e. they are free from IR-singularities and therefore can be computed unambiguously. A similar situation takes plays in B-decays [29, 30]. We can relate the amplitudes with the different  $J$  using the so-called physical subtraction scheme [29, 30]. Using Eqs.(46) and (47) in order to exclude colour-octet amplitude  $\mathcal{A}_J^{\perp(8)}$  one obtains

$$\mathcal{A}_1^\perp + \frac{1}{\sqrt{2}} \mathcal{A}_2^\perp = \mathcal{A}_1^{\perp(0)} + \frac{1}{\sqrt{2}} \mathcal{A}_2^{\perp(0)}. \quad (48)$$

The combination of the colour-singlet amplitudes in the *rhs* of this equation must be well defined since the *lhs* is free from any divergencies. This point can be easily verified using results in Eqs.(21). Performing the required analytical calculations we indeed obtain that the combination  $\mathcal{A}_1^{\perp(0)} + \frac{1}{\sqrt{2}} \mathcal{A}_2^{\perp(0)}$  is free from the endpoint divergencies. This observation supports the factorisation formula suggested in Eq.(47). Notice that this compensation works independently for two different collinear operators describing  $P_2 V_3$  and  $P_3 V_2$  projections. Relation (48) is one of the main results of this work and it will be used in our phenomenological analysis in Sec.5.

At the end of this section let us provide the analytical results for the collinear integrals which define

the symmetry breaking contributions in Eq.(48)

$$\begin{aligned}
\mathcal{A}_{1c}^{\perp(0)} + \frac{1}{\sqrt{2}}\mathcal{A}_{2c}^{\perp(0)} &\equiv \Delta\mathcal{A}_c^{\perp(0)} \\
&= \frac{i\langle\mathcal{O}({}^3P_J)\rangle}{m_c^3} \frac{f_P f_V^{\parallel} m_V}{m_c^3} \left(\frac{\pi\alpha_s}{N_c}\right)^2 C_F \sqrt{2} \left(J_c^{(1)}[P_2V_3] + J_c^{(2)}[P_2V_3]\right) \\
&\quad + \frac{i\langle\mathcal{O}({}^3P_J)\rangle}{m_c^3} \frac{f_P \mu_P f_V^{\perp}}{m_c^3} \left(\frac{\pi\alpha_s}{N_c}\right)^2 C_F \sqrt{2} \left(J_c^{(1)}[P_3V_2] + J_c^{(2)}[P_3V_2]\right). \quad (49)
\end{aligned}$$

Using the models of DAs from Appendix A we obtain

$$\begin{aligned}
J_c^{(1)}[P_2V_3] + J_c^{(2)}[P_2V_3] &= \frac{3}{2}b_1 \left\{ \frac{9}{4}(8 - \pi^2) + a_{2V}^{\parallel} \frac{9}{16}(11\pi^2 - 108) \right\} \\
&\quad + \frac{3}{2}b_1\lambda_s^+ \left[ \frac{9}{2}(8 - 3\zeta(3) + \pi^2(1 - 2\ln 2)) + 9a_{2V}^{\perp} \left( 9(1 - \zeta(3)) + \pi^2 \left( \frac{17}{4} - 6\ln 2 \right) \right) \right] \\
&\quad + \frac{3}{2}b_1\lambda_s^- a_{1V}^{\perp} \frac{27}{4}(6\zeta(3) - 24 + \pi^2(4\ln 2 - 1)) + \frac{3}{2}a_{1V}^{\parallel} \left\{ \frac{3}{4}(8 - \pi^2) + b_2 \frac{9}{8}(11\pi^2 - 108) \right\} \\
&\quad + \frac{3}{2}\lambda_s^- \left\{ -\frac{3}{4}[6\zeta(3) + 4\pi^2(\ln 2 - 1)] - \frac{9}{4}b_2(12\zeta(3) - 40 + \pi^2(8\ln 2 - 3)) \right. \\
&\quad \left. - a_{2V}^{\perp} \frac{3}{2} \left[ 18\zeta(3) - 40 + \pi^2(12\ln 2 - 7) + \frac{3}{2}b_2(72\zeta(3) + 300 + \pi^2(48\ln 2 - 73)) \right] \right\} \\
&\quad + \frac{3}{2} \left( -\frac{9}{8} \right) \lambda_s^+ a_{1V}^{\perp} \left\{ 2(6 - \zeta(3) - 8 + \pi^2(4\ln 2 - 3)) + b_2 [84 + \pi^2(48\ln 2 - 51) + 72\zeta(3)] \right\}, \quad (50)
\end{aligned}$$

$$J_c^{(1)}[P_3V_2] + J_c^{(2)}[P_3V_2] = -\frac{9}{8}\rho_-^K \left\{ 2\pi^2 + a_{2V}^{\perp} 3(20 - \pi^2) + b_2(20 - \pi^2 + a_{2V}^{\perp}(39\pi^2 - 360)) \right\}, \quad (51)$$

where we assume that all parameters of DAs depend on the factorisation scale  $\mu$ . From these results one can also see that in the limit of exact  $SU(3)$  symmetry expressions (50) and (51) vanish as it must be.

### 3.3 Soft-overlap colour-singlet contribution to amplitudes $\mathcal{A}_{1,2}^{\perp}$

There is one more contribution which can provide a significant effect and therefore must be taken into account. This contribution appears due to long distance interactions between the outgoing partons and can be associated with the typical hadronic scale  $\Lambda$ . In this case heavy quark and antiquark annihilate at short distances into the light quark-antiquark pair with the hard-collinear momenta  $p_{hc}^2 \sim m_c\Lambda$ . The light-cone fractions of these momenta are large and close to the total momenta of outgoing mesons. In order to produce final hadronic states the hard-collinear particles interact with the soft and collinear particles. Corresponding subprocess depends on the hard-collinear and soft virtualities which are of order  $m_c\Lambda$  and  $\Lambda^2$ , respectively. Such contribution can be described as a matrix element within the soft collinear effective theory (SCET) framework.

Corresponding diagrams are schematically shown in Fig.2(a), the dashed lines denote the hard-collinear particles which are attached to the blob denoting the SCET matrix element. We assume that the hard-collinear scale  $m_c\Lambda$  is not large and consider the SCET matrix elements as non-perturbative objects. If in the limit  $m_c \rightarrow \infty$  these matrix elements are of order  $(\Lambda/m_c)^3$  then the soft-overlap amplitude is of the same order as the hard one, see Eq.(30). This can be directly verified in SCET-II [26] by construction of the relevant  $T$ -products or by direct computation of the higher-order diagrams as in Fig.2(b). Such diagrams must have specific collinear endpoint singularities which can be associated with the SCET matrix elements. Such calculations are known for quite similar space-like amplitude describing the process  $\gamma^*\rho \rightarrow \pi$ , see e.g. Refs. [14, 32]. The detailed analysis of this point is quite complicated and we accept that power behaviour of the soft-overlap contribution like  $(\Lambda/m_c)^3$  as a reliable assumption.

The soft-overlap matrix elements describe a configuration when the outgoing hard-collinear partons carry almost total hadronic momentum. Such situation can be interpreted as a soft-overlap of the final

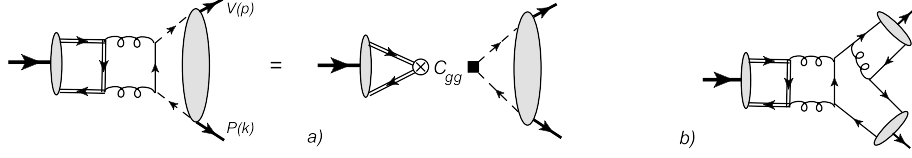


Figure 2: *a)* An example of the one-loop diagram and schematic factorisation for the soft-overlap colour-singlet contribution. The black square denotes the operator vertex and dashed fermion lines with the blob denote SCET matrix element defined in Eq.(53). The crossed vertex with the blob describe the NRQCD matrix element. *b)* The higher order perturbative diagram which must have IR-singularities associated with the soft-overlap configuration.

hadronic states. For space-like form factors such scattering configuration is also known as a Feynman mechanism [33] and corresponding effect has been studied long time ago with the help of the light-front wave functions [34].

The hard coefficient functions  $C_{gg}$  are given by the sum of the one-loop diagrams like one in Fig.2(a). The resulting expression for the colour-singlet soft-overlap amplitudes can be written as

$$\mathcal{M}_{\chi_{cJ} \rightarrow \bar{K}K^*} \Big|_{\text{Fig.2a}} \simeq \frac{i \langle \mathcal{O}({}^3P_J) \rangle}{m_c^3} C_{gg}^{(J)} \{ \delta_{J1} i \epsilon_{\rho\sigma}^\perp \epsilon_\chi^\sigma + \delta_{J2} (\epsilon_\chi)_{\rho\sigma} \bar{n}^\sigma \} \langle \bar{K}K^* | \mathcal{O}_{SCET} | 0 \rangle, \quad (52)$$

where  $\delta_{Ji}$  is Kronecker symbol, the matrix element of the two-particle SCET operator  $\mathcal{O}_{SCET}$  is defined as

$$\langle \bar{K}(k)K^*(p, e^*) | \bar{s}_{\bar{n}}(0)W_{\bar{n}}\gamma_\perp^\alpha W_n^\dagger s_n(0) - \bar{q}_n(0)W_n\gamma_\perp^\alpha W_{\bar{n}}^\dagger q_{\bar{n}}(0) | 0 \rangle = i \epsilon_{\alpha\beta}^\perp (e^*)^\beta m (f_{PV}^s - f_{PV}^q). \quad (53)$$

Here the quark fields  $\psi_n, \psi_{\bar{n}}$  ( $\psi = s, q$ ) and  $W_{n,\bar{n}}$  denote the hard-collinear SCET fields and corresponding hard-collinear Wilson lines

$$\not{n}\psi_n(x) = 0, \quad W_n = P \exp \left\{ ig \int_{-\infty}^0 ds \bar{n} \cdot A(s\bar{n}) \right\}, \quad (54)$$

and similarly for the light-cone sector associated with  $\bar{n}$ .

The form factors  $f_{PV}^{s,q}$  describe transition of the hard-collinear quark-antiquark pair to the final hadronic state within the SCET framework. The relative sign minus in Eq.(53) can be understood as an consequence of  $C$ -parity of the initial state. We see that in the exact  $SU(3)$  limit such matrix element vanishes as it must be. The definition (53) is process independent, the similar matrix element may also appear in other hard reactions, for instance, in the wide angle scattering  $\gamma\gamma \rightarrow \bar{K}K^*$  at large energy and momentum transfer. The different combination of these form factors can also appear in the process  $e^+e^- \rightarrow \gamma^* \rightarrow \bar{K}K^*$ . Using Eqs.(52) and (53) one can easily find corresponding contributions to the colour-singlet amplitudes  $\mathcal{A}_J^{\perp(0)}$

$$\mathcal{A}_{Js}^{\perp(0)} = \frac{i \langle \mathcal{O}({}^3P_1) \rangle}{m_c^3} C_{gg}^{(J)} (f_{PV}^s - f_{PV}^q). \quad (55)$$

The computation of the hard coefficients  $C_{gg}^{(J)}$  is straightforward: one has to compute the box diagrams as in Fig.2(a) in the appropriate kinematics. The required one-loop integrals are similar to the integrals studied for  $\chi_{cJ} \rightarrow e^+e^-$  decays. We borrow the results from Refs. [35] adding the colour factor and QCD couplings. These integrals have IR-divergencies which are regularised by dimensional regularisation  $D = 4 - 2\epsilon$ . Using  $\overline{MS}$ -scheme one obtains

$$C_{gg}^{(J=1)} = \alpha_s^2 \frac{C_F}{N_c} \frac{1}{\sqrt{2}} \left( -\frac{1}{\epsilon} - \ln \frac{\mu^2}{m_c^2} - 2 \ln 2 \right), \quad C_{gg}^{(J=2)} = \alpha_s^2 \frac{C_F}{N_c} \left\{ \frac{1}{\epsilon} + \ln \frac{\mu^2}{m_c^2} + \frac{2}{3} (\ln 2 - 1 + i\pi) \right\}, \quad (56)$$

where  $\mu$  is the factorisation scale. The IR-singularities in the hard loop corresponds to the integration domain where one of the gluons becomes ultrasoft. Corresponding IR-poles can be again absorbed into

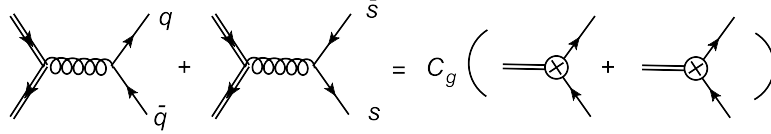


Figure 3: The hard factorisation associated with the annihilation  $c\bar{c} \rightarrow g^* \rightarrow q(s) + \bar{q}(\bar{s})$ . The crossed circle denotes the vertex of the four-fermion operator and the attached double line describes the heavy quark-antiquark pair.

the colour-octet matrix element which will be discussed this in Sec. 4. The total result for a soft-overlap amplitude is also given by the sum of colour-singlet and colour-octet matrix elements.

The soft-overlap colour-octet contribution also satisfies Eq.(46) as a part of the total colour-octet amplitude. Therefore one can also apply the same arguments and obtain the relation like Eq.(48) which allows one to define the corresponding HQSS breaking terms. Using Eq.(56) we obtain

$$\mathcal{A}_{1s}^{\perp(0)} + \frac{1}{\sqrt{2}}\mathcal{A}_{2s}^{\perp(0)} \equiv \Delta\mathcal{A}_s^{\perp(0)} = \frac{i\langle\mathcal{O}({}^3P_2)\rangle}{m_c^3} (f_{PV}^s - f_{PV}^q) \alpha_s^2 \frac{C_F}{N_c} \frac{\sqrt{2}}{3} (-1 - 2\ln 2 + i\pi). \quad (57)$$

We again confirm that IR-poles and factorisation scale cancel as it is expected. Notice that this contribution has imaginary part which is related to the two-gluon intermediate cut in the loop diagram. This contribution is also of order  $\alpha_s^2$  and have the same power counting behaviour as  $\mathcal{A}_{\perp}^{(0)}$  in Eq.(49). If the value of the SCET matrix elements  $\sim (f_{PV}^s - f_{PV}^q)$  is sufficiently large then this contribution cannot be neglected.

## 4 Colour-octet contributions in the Coulomb limit

For a realistic charmonium colour-octet matrix elements can be computed only within a non-perturbative framework. However in order to study certain properties of the NRQCD matrix elements it could be useful to consider a special limit, also known as the Coulomb limit, when the ultrasoft scale is sufficiently large. In such limit the ultrasoft scale is a larger than the typical hadronic scale  $m_c v^2 \gg \Lambda$  and quarkonium state can be considered as a weakly bound state with the binding energy  $E \sim m_c v^2$ . Important point is that the perturbation theory can be used for calculations associated with the ultrasoft scale. The standard framework includes: factorisation of hard modes and transition to NRQCD, the integration over the soft and potential gluons and transition to pNRQCD which only contains potential heavy quarks and ultrasoft gluons as degrees of freedom. Such picture of course cannot provide reliable estimates for realistic charmonia but it allows one to study a structure of the infrared divergencies which are related with the mixing of colour-singlet and -octet operators. Our aim is to show that the colour-octet matrix elements satisfy to Eq.(46) in the Coulomb limit and to study UV- and IR-singularities in the colour-singlet and -octet contributions.

In our case the factorisation of hard modes is described by the tree level diagrams associated with the subprocess  $c\bar{c} \rightarrow g^* \rightarrow q + \bar{q}$  or  $c\bar{c} \rightarrow g^* \rightarrow s + \bar{s}$  as shown graphically in Fig. 3. Two diagrams correspond to the two different regions  $y \sim \bar{x} \sim v^2$  or  $x \sim \bar{y} \sim v^2$  in the collinear integrals. Hence for the octet amplitudes we get

$$i\mathcal{M}_{\chi_{cJ} \rightarrow K^* \bar{K}}^{(8)} = C_g \langle K^* \bar{K} | \{ \bar{s}_{\bar{n}}(0) W_{\bar{n}} \gamma_{\perp}^{\alpha} t^a W_n^{\dagger} s_n(0) + \bar{q}_{\bar{n}}(0) W_{\bar{n}} \gamma_{\perp}^{\alpha} t^a W_n^{\dagger} q_n(0) \} \chi_{\omega}^{\dagger} \gamma_{\perp}^{\alpha} t^a \psi_{\omega} | \chi_{cJ} \rangle, \quad (58)$$

with the hard coefficient function

$$C_g = \frac{i\alpha_s(\mu)\pi}{m_c^2}. \quad (59)$$

In Eq.(58) we also use notation for the collinear fields and Wilsons lines as in Eq.(54).

The next step is transition to pNRQCD. To our accuracy the matching of the NRQCD operator in (58) onto pNRQCD operator is trivial

$$\chi_{\omega}^{\dagger} \gamma_{\perp}^{\alpha} t^a \psi_{\omega} |_{NRQCD} = \chi_{\omega}^{\dagger} \gamma_{\perp}^{\alpha} t^a \psi_{\omega} |_{pNRQCD}. \quad (60)$$

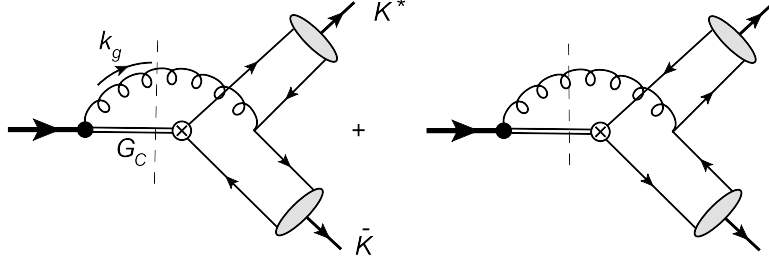


Figure 4: The diagrams in pNRQCD describing the colour-octet matrix elements. The double line denotes the colour-octet Coulomb propagator  $G_C$ . The dashed line shows the cut associated with the imaginary part.

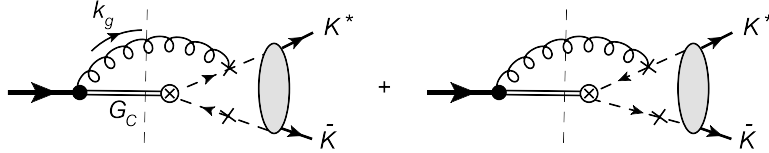


Figure 5: The one-loop pNRQCD diagrams describing the colour-octet matrix elements with the soft-overlap matrix element. The crossed quark lines indicate all possible attachments of the ultrasoft gluon.

Therefore we can easily pass to a calculation of the matrix element (58) in pNRQCD.

To the leading-order accuracy in  $\alpha_s$  one can consider two different sets of Feynman diagrams: tree level and one-loop graphs which are shown in Fig. 4 and Fig. 5.

The tree diagrams in Fig. 4 have the following structure. The initial  $P$ -wave bound state decays through the chromoelectric dipole interaction into ultrasoft gluon and bound quark-antiquark pair in the colour-octet state. The interaction vertex is suppressed by power of the small velocity  $v$  therefore the total octet contribution is of order  $v^4$  (remind, the  $S$ -wave vector operator in (58) is of order  $v^3$ ). The colour-octet quark-antiquark pair propagates a distance  $\sim 1/(m_c v^2)$  and annihilates into light quark-antiquark pair with momenta of order  $k$  and  $p$ . The colour-octet propagator is described by the non-relativistic Coulomb Green function  $G_C$ . The virtual ultrasoft gluon also creates the light quark-antiquark pair which together with the collinear quark-antiquark provide a collinear operator describing a long distance overlap with outgoing mesonic states. Since  $p_{us}^2 \gg \Lambda^2$  the ultrasoft particles still can be matched onto collinear degrees of freedom. However the corresponding collinear fractions are small, of order  $v^2$  as it follows from the momentum conservation. Therefore corresponding collinear matrix elements describe an asymmetric collinear configurations where one parton carries the small collinear fraction  $x \sim v^2$ . This is exactly the endpoint configuration which provides the IR-singularities in the colour-singlet matrix element. The resulting expression for such diagram must be expanded with respect to small collinear fractions keeping only those terms which provide contribution of order  $v^4$ . The long distance dynamics associated with the hadronic scale  $\Lambda$  is still described by the DAs originating from the collinear matrix elements. Such situation is a consequence of presence of the two well separated scales  $m_c v^2 \gg \Lambda$  in the Coulomb limit.

The one-loop diagrams in Fig. 5 describe the colour-octet contribution associated with the soft-overlap amplitude. In this case the ultrasoft gluon interacts with the collinear quark or antiquark creating the colourless quark-antiquark operator. Further interactions of the hard-collinear particles is only associated with the typical hadronic scale  $\Lambda$  and described as matrix elements of the SCET operator which is shown by blob in Fig.5. As in Sec. 3 we consider these matrix elements as non-perturbative quantities. Obviously, such contribution also is of order  $v^4$ .

Technically the calculation of the pNRQCD diagrams in Fig.4 is similar to calculation in Ref. [31] and useful technical details can be found in this work. The analytical expression for the colour-octet

amplitude can be written as

$$\begin{aligned} \mathcal{M}_{\chi_{cJ} \rightarrow K^* \bar{K}}^{(8)} \Big|_{\text{Fig.4}} &= -\frac{2\pi^2}{m_c^2} \alpha_s(\mu_{us}) \alpha_s(\mu) \frac{C_F}{N_c^2} \\ &\int_0^1 dx \int_0^1 dy \left( \frac{\theta(\bar{x} < \eta) \theta(y < \eta)}{(yk + \bar{x}p)^2} D_s^{\alpha\beta}(x, y) + \frac{\theta(x < \eta) \theta(\bar{y} < \eta)}{(\bar{y}k + xp)^2} D_q^{\alpha\beta}(x, y) \right) \\ &\times \sqrt{N_c} \sqrt{M_\chi} \sqrt{\frac{3}{4\pi}} \int \frac{d^3 \vec{\Delta}}{(2\pi)^3} \tilde{R}_{21}(\Delta) \frac{1}{4} \text{tr} [\Lambda_J (1 - \psi) \gamma_{\perp\alpha} (1 + \psi)] D_Q^\beta(E, \Delta_\top). \end{aligned} \quad (61)$$

The second line of Eq.(61) describes the subdiagram with light quarks and ultrasoft gluon propagators (which gives expressions in the denominators). The  $\theta$  functions restrict the integrations regions over the quark collinear fractions and cut-off  $\eta$  must be understood as UV-regulator. The functions  $D_s$  and  $D_q$  consist of contributions of the light-quark vertices and DAs. A calculation of these contributions is the same as for the colour-singlet case but in addition one has to expand the integrands with respect to small fractions in the regions  $y \sim \bar{x} \sim v^2$  or  $x \sim \bar{y} \sim v^2$  as it is indicated by the appropriate  $\theta$ -functions.

The third line in Eq.(61) describes the heavy quark subdiagram. The relative heavy quark momentum  $\Delta_\top$  is of order  $m_c v$ , in what follow we assume that  $\Delta \equiv |\vec{\Delta}|$ . The momentum space radial wave function of  $P$ -wave state reads

$$\tilde{R}_{21}(\Delta) = iR'_{21}(0) \frac{16\pi\gamma_B\Delta}{(\Delta^2 + \gamma_B^2/4)^3}, \quad \gamma_B = \frac{1}{2} m_c \alpha_s C_F. \quad (62)$$

where  $R'_{21}(0)$  is the derivative of the position radial wave function at the origin. The trace over Dirac indices includes the projectors on  $P$ -wave state

$$\Lambda_1 = \frac{1}{2\sqrt{2}} \frac{\Delta_\top^\rho}{\Delta} [\gamma_\rho, \not{\epsilon}_\chi] \gamma_5, \quad \Lambda_2 = -\epsilon^{\mu\nu} \frac{\Delta_\top^\mu}{\Delta} \gamma_{\top\nu}. \quad (63)$$

The factor  $\gamma_{\perp\alpha}$  originates from the vertex of the octet  $S$ -wave operator in Eq.(58). A simple calculation yields

$$\frac{1}{4} \text{tr} [\Lambda_J (1 - \psi) \gamma_{\perp\alpha} (1 + \psi)] = -\frac{\Delta_\top \cdot (n - \bar{n})}{\Delta} \frac{1}{2} \left( \delta_{J1} \sqrt{2} i \epsilon_{\rho\alpha}^\perp \epsilon_\chi^\rho + \delta_{J2} 2(\epsilon_\chi)_{\alpha\perp\beta} \bar{n}^\beta \right). \quad (64)$$

The expression in the brackets in Eq.(64) gives the dependence on the total momentum  $J$  in the amplitude (61). The function  $D_Q^\beta(E, \Delta_\top)$  in Eq.(61) is described by the chromoelectric vertex generated from the pNRQCD interaction Lagrangian

$$\mathcal{L}_{int}(x) = -g\psi_\omega^\dagger(x) \vec{x} \cdot \vec{E}(t) \psi_\omega(x) - g\chi_\omega^\dagger(x) \vec{x} \cdot \vec{E}(t) \chi_\omega(x), \quad (65)$$

and by octet Coulomb Green function  $G_C$

$$D_Q^\beta(E, \Delta_\top) = (\omega^\beta k_g^\lambda - g_\top^{\beta\lambda}(\omega k_g)) \frac{\partial}{\partial \Delta_\top^\lambda} \int \frac{d^3 \vec{\Delta}'}{(2\pi)^3} G_C(\Delta_\top, \Delta'_\top; E - (\omega k_g)), \quad (66)$$

where  $k_g$  denotes the outgoing ultrasoft gluon momentum ( remind that  $k_g = yk + \bar{x}p$  for the  $D_s^{\alpha\beta}$  and  $k_g = \bar{y}k + xp$  for  $D_q^{\alpha\beta}$  ). The expression for the Coulomb Green function is obtained by summation of the ladder diagrams with the colour-octet potential insertions. The resulting expression is quite complicated

$$G_{(8)}(\Delta_\top, \Delta'_\top; E) = -\frac{(2\pi)^3 \delta^{(3)}(\vec{\Delta} - \vec{\Delta}')}{E + \Delta_\top^2/m_c} + \frac{g^2}{2N_c} \frac{1}{E + \Delta_\top^2/m_c} \frac{1}{(\vec{\Delta} - \vec{\Delta}')^2} \frac{1}{E + \Delta_\top'^2/m_c} + \mathcal{O}(g^4). \quad (67)$$

The full expression can be found in Refs. [45, 46]. In the various calculations, see e.g. Refs. [31, 47–49], it has been observed that the dominant numerical impact is provided by the relatively simple first term in Eq.(67), while the remnant higher order contributions are suppressed by the factor  $1/(2N_c)$  for each

colour-octet exchange. For our purpose it is also enough to consider an approximation which is given by no-gluon exchange leading term in Eq.(67). This gives

$$D_Q^\beta(E, \Delta_\top) \simeq (\omega^\beta k_g^\lambda - g_\top^{\beta\lambda}(\omega k_g)) \frac{2\Delta_\top^\lambda}{m_c} \frac{1}{[E - (\omega k_g) + \Delta_\top^2/m_c + i\varepsilon]^2}, \quad (68)$$

Substituting (64) and (68) into Eq.(61), and using rotation invariance in order to reduce  $\Delta_\top^\rho \Delta_\top^\lambda \rightarrow -\Delta^2 g_\top^{\rho\lambda}/3$  one obtains

$$\begin{aligned} \mathcal{M}_{\chi_{cJ} \rightarrow K^* \bar{K}}^{(8)} \Big|_{\text{Fig.4}} &= \left( \delta_{J1} \sqrt{2} i \varepsilon_{\rho\alpha}^\perp \epsilon_\chi^\rho + \delta_{J2} 2(\epsilon_\chi)_{\alpha\rho} \bar{n}^\rho \right) \frac{-2\pi^2}{m_c^2} \alpha_s(\mu_{us}) \alpha_s(\mu) \frac{C_F}{N_c^2} \\ &\int_0^1 dx \int_0^1 dy \left( \frac{\theta(\bar{x} < \eta) \theta(y < \eta)}{(yk + \bar{x}p)^2} D_s^{\alpha\beta}(x, y) + \frac{\theta(x < \eta) \theta(\bar{y} < \eta)}{(\bar{y}k + xp)^2} D_q^{\alpha\beta}(x, y) \right) \\ &\times \sqrt{N_c} \sqrt{M_\chi} \sqrt{\frac{3}{4\pi}} \frac{1}{m_c} \int \frac{d^3 \vec{\Delta}}{(2\pi)^3} \tilde{R}_{21}(\Delta) \frac{\Delta}{3} \frac{\bar{n}^\beta(nk_s) - n^\beta(\bar{n}k_s)}{[E - (\omega k_g) + \Delta_\top^2/m_c + i\varepsilon]^2}. \end{aligned} \quad (69)$$

Notice that the total momentum  $J$  only enters in expression in the brackets in the first line. The Dirac traces in  $D_{s,q}^{\alpha\beta}$  allows one to conclude that the expression in Eq.(69) can be presented in the following form

$$\mathcal{M}_{\chi_{cJ} \rightarrow K^* \bar{K}}^{(8)} \Big|_{\text{Fig.4}} = \{ \delta_{J1} \sqrt{2} i \varepsilon_{\rho\alpha}^\perp \epsilon_\chi^\rho + \delta_{J2} 2(\epsilon_\chi)_{\alpha\beta} \bar{n}^\beta \} (-i) \varepsilon_\perp^{\alpha\rho} (e_V^*)_\rho m_c J_{us} \quad (70)$$

$$= \{ \delta_{J1} (\epsilon_\chi e_V^*) - \delta_{J2} (\epsilon_\chi)_{\alpha\beta} \bar{n}^\beta i \varepsilon_\perp^{\alpha\rho} (e_V^*)_\rho \} m_c (-1)^J 2^{J/2} J_{us}, \quad (71)$$

where  $J_{us}$  is the universal convolution integral. Comparing the last equation with the definitions of the scalar amplitudes in Eqs.(10) and (11) one obtains

$$\mathcal{A}_{Jc}^{\perp(8)} = (-1)^J 2^{J/2} J_{us}. \quad (72)$$

This result already gives the relation in Eq.(46). In order to obtain Eq.(72) we used the approximate expression for the Coulomb Green function but the given derivation can also be extended to the case of exact colour-octet propagator.

For the ultrasoft integral we obtain

$$J_{us} = \frac{i \langle \mathcal{O}^3 P_J \rangle}{m_c^3} \alpha_s(\mu) \alpha_s(\mu_{us}) \frac{\pi^2}{N_c^2} C_F \left( \frac{f_V^\perp f_P \mu_P}{m_c^3} J_{us}[P_3 V_2] + \frac{f_P f_V m_V}{m_c^3} J_{us}[P_2 V_3] \right), \quad (73)$$

with

$$J_{us}[P_3 V_2] = m_c^2 \mathcal{N} \int \frac{d^3 \vec{\Delta}}{(2\pi)^3} \tilde{R}_{21}(\Delta) \Delta \int_{1-\eta}^1 dx \int_0^\eta dy \frac{\bar{\phi}_{2V}^{\perp\prime}(1) \Delta \phi_{3P}^p(y \sim 0) + \Delta \phi_{2V}^{\perp\prime}(1) \bar{\phi}_{3P}^p(y \sim 0)}{[E - m_c(y + \bar{x}) + \Delta_\top^2/m_c + i\varepsilon]^2}, \quad (74)$$

$$J_{us}[P_2 V_3] = \frac{m_c^2}{2} \mathcal{N} \int \frac{d^3 \vec{\Delta}}{(2\pi)^3} \tilde{R}_{21}(\Delta) \Delta \int_{1-\eta}^1 dx \int_0^\eta dy \frac{\bar{\phi}'_{2P}(0) (I[\Delta\Omega] - \Delta\Omega(1) \ln \bar{x}) + \Delta \phi'_{2P}(0) I[\bar{\Omega}]}{[E - m_c(y + \bar{x}) + \Delta_\top^2/m_c + i\varepsilon]^2}. \quad (75)$$

where normalisation factor  $\mathcal{N}$  is defined as

$$\mathcal{N} = \frac{1}{3} \frac{1}{i R'_{21}(0)}, \quad \mathcal{N} \int \frac{d^3 \vec{\Delta}}{(2\pi)^3} \tilde{R}_{21}(\Delta) \Delta = 1. \quad (76)$$

In Eq.(75) we also defined the short notation

$$I[f] = \int_0^1 du \frac{f(u) - f(1)}{1 - u}. \quad (77)$$

Remind that functions  $\bar{f}$  and  $\Delta f$  denote symmetric and antisymmetric components, see Eq.(23).

The ultrasoft integrals in Eqs.(74) and (75) are divergent if one takes UV cut-off  $\eta \rightarrow \infty$ . In order to compute these integrals we must use the same regularisation as for the colour-singlet case. Therefore we introduce the analytical regularisation substituting

$$\frac{1}{[E - m_c(y + \bar{x}) + \Delta_\uparrow^2/m_c + i\varepsilon]^2} \rightarrow \frac{\nu^{2\varepsilon}}{[E - m_c(y + \bar{x}) + \Delta_\uparrow^2/m_c + i\varepsilon]^{2+\varepsilon}} \quad (78)$$

and then take the limit  $\eta \rightarrow \infty$ . Remind, that in Eq.(78) we assume  $y \sim \bar{x} \sim v^2$  and therefore all terms in the denominator are of order  $mv^2$ .

Consider as example the following term from Eq.(74)

$$J_{us1}[P_2V_3] = m_c^2 \mathcal{N} \int \frac{d^3 \vec{\Delta}}{(2\pi)^3} \tilde{R}_{21}(\Delta) \Delta \int_{-\infty}^1 dx \int_0^\infty dy \frac{\nu^{2\varepsilon} \bar{\phi}_{2V}^{\perp\prime}(1) \Delta \phi_{3P}^p(y \sim 0)}{[E - m_c(y + \bar{x}) + \Delta_\uparrow^2/m_c + i\varepsilon]^{2+\varepsilon}}. \quad (79)$$

Performing expansion of the integrand in the UV-region  $y \sim \bar{x} \rightarrow \infty$  one can see the overlap with the singular collinear integral in Eq.(39). The regularised integral in Eq.(79) can be easily computed separating the divergent part in the following way

$$\begin{aligned} J_{us1}[P_3V_2] &= m_c^2 \mathcal{N} \int \frac{d^3 \vec{\Delta}}{(2\pi)^3} \tilde{R}_{21}(\Delta) \Delta \int_0^\infty dx \int_0^\infty dy \left( \bar{\phi}_{2V}^{\perp\prime} \right)'(1) \Delta \phi_{3P}^p(y \sim 0) \\ &\times \left( \frac{1}{[E - m_c(y + x) + \Delta_\uparrow^2/m_c + i\varepsilon]^2} - \frac{1}{[E - m_c(y + x) + i\varepsilon]^2} \right) \\ &+ m^2 \int_0^\infty dx \int_0^\infty dy \frac{\nu^{2\varepsilon} \bar{\phi}_{2V}^{\perp\prime}(1) \Delta \phi_{3P}^p(y \sim 0)}{[E - m_c(y + x) + i\varepsilon]^{2+\varepsilon}}, \end{aligned} \quad (80)$$

where we used relation (76). The first integral in (80) is finite and therefore the regularisation in this case can be omitted. Then the integrals over the collinear fractions can be easily computed and one finds ( $t = \nu^2/m_c^2$ )

$$\begin{aligned} J_{us1}[P_3V_2] &= \bar{\phi}_{2V}^{\perp\prime}(1) \frac{3}{2} \rho_-^K \left\{ \frac{\beta}{\varepsilon^2} + \frac{1}{\varepsilon} (\beta \ln t + \alpha - \beta) + \frac{\beta}{2} \ln^2 t + (\beta - \alpha)(1 - \ln t) - \beta \frac{\pi^2}{6} \right. \\ &\left. - \mathcal{N} \int \frac{d^3 \vec{\Delta}}{(2\pi)^3} \tilde{R}_{21}(\Delta) \Delta \left( \frac{1}{2} \beta \ln^2 [\Delta^2/m_c^2 - E/m_c - i0] + \alpha \ln [\Delta^2/m_c^2 - E/m_c - i0] \right) \right\}, \end{aligned} \quad (81)$$

with  $\alpha$  and  $\beta$  defined in Eq.(33). Comparing this result with the expression in Eq.(43) one can see that the poles and logarithms  $\ln t$  cancel in the sum  $J_{c1}^{(J)}[P_2V_3] + (-1)^J J_{us1}[P_2V_3]$ . The computation of the other integrals in Eqs.(74) and (75) is similar, we have checked that the poles and  $\mu$ -dependence also cancel in the sum of singlet and octet amplitudes. This demonstrates that our matching is consistent and the endpoint IR singularities in the colour-singlet amplitude can be absorbed into colour-octet contribution. Therefore at least to a given accuracy the sum of the singlet and octet amplitudes describes the physical amplitude consistently.

The octet integrals in Eqs.(74) and (75) include the derivatives of DAs and integrals with the radial wave function as in Eq.(81). Such integrals generate imaginary part which appears from the region where  $\Delta^2/m_c < E$  and can be associated with the cut of diagrams as shown in Fig.4. The imaginary part is a direct consequence of the intermediate colour-octet state. The expression (81) also demonstrates that octet contribution is sensitive to the shape of the radial wave function  $\tilde{R}_{21}$  while the singlet amplitude depends only from the wave function at the origin. This is qualitative difference between the two terms and it is interesting to study, at least qualitatively, how this point can affect a description of quarkonium decays.

Consider now the diagrams in Fig. 5. Their computation can be done within the same technique as described above. The coupling of the ultrasoft gluon to the hard-collinear quarks is described by the



leading-order SCET interactions  $\bar{\psi}_n(x)g(n \cdot A_{us}((x\bar{n})n/2))\not{n}/2\psi_n(x)$  and similarly for the  $\bar{n}$  light-cone sector. This again yields the result (72) for the corresponding amplitudes

$$\mathcal{A}_{J_s}^{\perp(8)} = (-1)^J 2^{J/2} \tilde{J}_{us}. \quad (82)$$

The ultrasoft integral in this case reads

$$\begin{aligned} \tilde{J}_{us} &= \frac{i \langle \mathcal{O}({}^3P_0) \rangle}{m_c^3} \alpha_s(\mu_h) \alpha_s(\mu_{us}) \frac{C_F}{2N_c} (f_{PV}^s - f_{PV}^q) \mathcal{N} \int d^3\vec{\Delta} \tilde{R}_{21}(\Delta) \Delta \\ &\times \frac{1}{i\pi^2} \int d^D l \frac{1}{[l^2] [E - m_c(l\omega) + \Delta_\perp^2/m_c + i\varepsilon]^2}. \end{aligned} \quad (83)$$

The integral over the ultrasoft momentum  $l$  is UV-divergent and we use dimensional regularisation as before, with  $d^D l = e^{\varepsilon(\gamma_E + \ln \pi)} \mu_{us}^{2\varepsilon} d^{4-2\varepsilon} l$ . Calculation of this integral yields

$$\frac{1}{i\pi^2} \int d^D l \frac{1}{[l^2] [E - m_c(l\omega) + \Delta_\perp^2/m_c + i\varepsilon]^2} = -\frac{1}{\varepsilon} + \ln \frac{m_c^2}{\mu^2} + 2 \ln[2(\Delta^2/m_c - E - i0)/m_c]. \quad (84)$$

Therefore we obtain

$$\begin{aligned} A_{J=2,s}^{\perp(8)} &= 2\tilde{J}_{us} = \frac{i \langle \mathcal{O}({}^3P_0) \rangle}{m_c^3} \alpha_s(\mu) \alpha_s(\mu_{us}) \frac{C_F}{N_c} (f_{PV}^s - f_{PV}^q) \\ &\times \left( -\frac{1}{\varepsilon} + \ln \frac{m_c^2}{\mu^2} + 2 \ln 2 + 2\mathcal{N} \int \frac{d^3\vec{\Delta}}{(2\pi)^3} \tilde{R}_{21}(\Delta) \Delta \ln[(\Delta^2/m_c - E - i0)/m_c] \right). \end{aligned} \quad (85)$$

Comparing this expression with the hard contribution in (56) we observe that poles in  $1/\varepsilon$  and  $\mu$ -dependence cancel in the sum  $A_{J,s}^{\perp(0)} + A_{J,s}^{\perp(8)}$ . The soft-overlap amplitude (85) also has imaginary part which is generated by the cut shown in Fig.5.

To summarise. The colour-octet amplitudes defined in Eq.(58) are given by the sum

$$\mathcal{A}_J^{\perp(8)} = \mathcal{A}_{J_c}^{\perp(8)} + \mathcal{A}_{J_s}^{\perp(8)}. \quad (86)$$

The total decay amplitudes are given by the sum of the singlet and octet amplitudes (47), the singular terms cancel in this sum so that decay amplitude is well defined. This cancellation allows us conclude that various IR-singularities which have been observed in the colour-singlet amplitudes can be absorbed into renormalisation of the colour-octet matrix element (58). This matrix element is sensitive to a long-distance behaviour of the quarkonium wave function and have imaginary part due to long distance interactions. Can one get any information about the colour-octet contribution from the experimental data? We try to study this question in the next section.

## 5 Phenomenology

In Sec.3 we obtained that the colour-singlet amplitude  $\mathcal{A}_1^{\parallel}$  provides a tiny contribution and cannot describe the measured branching ratio. Hence we can suppose that the dominant effect is provided by the transverse amplitudes which are given by the sum of the colour-singlet and colour-octet terms. Suppose that the largest numerical effect is provided by the colour-octet amplitudes  $\mathcal{A}_J^{\perp(8)}$ , i.e.  $\mathcal{A}_J^{\perp(8)} \gg \mathcal{A}_J^{\perp(0)}$ . In the previous section it was established that these amplitude satisfy to Eq.(46) up to relativistic corrections in velocity  $v$ . Using this relation and Eqs.(14) and (15) one obtains

$$R_{th} = \frac{\Gamma[\chi_{c2} \rightarrow \bar{K}^0 K^{*0} + c.c.]}{\Gamma[\chi_{c1} \rightarrow \bar{K}^0 K^{*0} + c.c.]} \simeq \left(1 - \frac{m_P^2}{k_0^2}\right) \left(1 - \frac{m_P^2 m_V^2}{(kp)^2}\right) \frac{1}{5} \frac{3}{2} \frac{|\mathcal{A}_2^{(8)}|^2}{|\mathcal{A}_1^{(8)}|^2} = 0.55, \quad (87)$$

This estimate includes contribution from the model dependent power suppressed coefficient which yields

$$\left(1 - \frac{m_P^2}{k_0^2}\right) \left(1 - \frac{m_P^2 m_V^2}{(kp)^2}\right) = 0.91. \quad (88)$$

Using the data for neutral mesons  $\bar{K}^0$  and  $K^{*0}$  from Table 1 one finds

$$R_{\text{exp}} = \frac{\text{Br}[\chi_{c2} \rightarrow \bar{K}K^* + c.c.] \Gamma_{\text{tot}}[\chi_{c2}]}{\text{Br}[\chi_{c1} \rightarrow \bar{K}K^* + c.c.] \Gamma_{\text{tot}}[\chi_{c1}]} = 0.30 \pm 0.13, \quad (89)$$

where we used  $\Gamma_{\text{tot}}[\chi_{c1}] = 0.84$  MeV and  $\Gamma_{\text{tot}}[\chi_{c2}] = 1.93$  MeV [11]. The difference of about factor two between the values  $R_{\text{th}}$  and  $R_{\text{exp}}$  allows one to suppose that effect from the colour-singlet contribution is not negligible and could help to improve the description. For simplicity we consider only branching fractions of the neutral mesons. The decay amplitudes of the neutral and charged mesons must be the same due to  $SU(2)$  flavour symmetry and data support this conclusion. Therefore a consideration of the decays of charged mesons provides the similar results.

The colour-singlet HQSS breaking relations have been obtained in Eqs.(49) and (57). Using them we can relate the decay amplitudes as

$$\mathcal{A}_1^\perp = \Delta\mathcal{A}_c^{\perp(0)} + \Delta\mathcal{A}_s^{\perp(0)} - \frac{1}{\sqrt{2}}\mathcal{A}_2^\perp. \quad (90)$$

The absolute value  $|\mathcal{A}_2^\perp|$  can be estimated from the width  $\Gamma[\chi_{c2} \rightarrow \bar{K}^0 K^{*0} + c.c.]$  that gives

$$|\mathcal{A}_2^\perp| = (7.0 \pm 1.5) \times 10^{-3}. \quad (91)$$

The result for absolute value  $|\mathcal{A}_1^\perp|$  which can be obtained from Eq.(90) depends on the unknown imaginary phase of amplitude  $\mathcal{A}_2^\perp$

$$\mathcal{A}_2^\perp = |\mathcal{A}_2^\perp| e^{i\delta}, \quad (92)$$

and on the unknown difference of the SCET amplitudes  $f_{PV}^s - f_{PV}^q$  in  $\Delta\mathcal{A}_s^{\perp(0)}$ , see Eq.(85). We accept these quantities as unknown parameters. Let us rewrite the soft-overlap combination as

$$f_{PV}^s - f_{PV}^q = \frac{f_P f_V^\parallel m_V}{m_c^3} \Delta f, \quad (93)$$

where factor  $f_P f_V^\parallel m_V / m_c^3$  introduces a ‘‘natural’’ scale. In the following we assume that parameter  $\Delta f$  is real. We can not provide a rigorous arguments about a suppression of the imaginary part of  $\Delta f$  and therefore accept this simplification as reliable assumption.

In order to get numerical estimates we use the following non-perturbative input. The models of  $K$ -meson DAs, quark masses and numerical estimates for NRQCD matrix elements are described in Appendix A. Calculating symmetry breaking corrections  $\Delta\mathcal{A}_{Jc,s}^{\perp(0)}$  we use  $n_f = 4$ ,  $m_c = 1.5$  GeV and set the value of renormalisation scale  $\mu^2 = 2m_c^2$  that gives  $\alpha_s(2m_c^2) = 0.29$ . We also apply the leading logarithmic evolution for the parameters of DAs.

The expression for  $\Delta\mathcal{A}_c^{\perp(0)}$  is described in Eqs.(49)-(51) and using the numerical values of the DA parameters we obtain

$$\Delta\mathcal{A}_c^{\perp(0)} = (-1.56 \pm 0.19) \times 10^{-3}, \quad (94)$$

where the errors give the uncertainty from the variation of values of the DA parameters. Both contributions in Eq.(49) are negative, the largest numerical impact is provided by the terms proportional to  $SU(3)$ -breaking parameters  $\rho_-^K$  and  $\lambda_s^-$ , see definitions in Eqs.(108) and (118). The chiral enhanced contribution associated with the projection  $P_3V_2$  is about factor two larger than the contribution from the  $P_2V_3$  projection. Comparing results for amplitude  $|\mathcal{A}_2^\perp|$  in Eq.(91) and for  $\Delta\mathcal{A}_c^{\perp(0)}$  in Eq.(94) one finds that the value of the symmetry breaking corrections are few times smaller.

For the symmetry breaking soft-overlap contribution (57) we obtain

$$\Delta\mathcal{A}_s^{\perp(0)} = (-0.10 + 0.13i) \Delta f \times 10^{-3}, \quad (95)$$

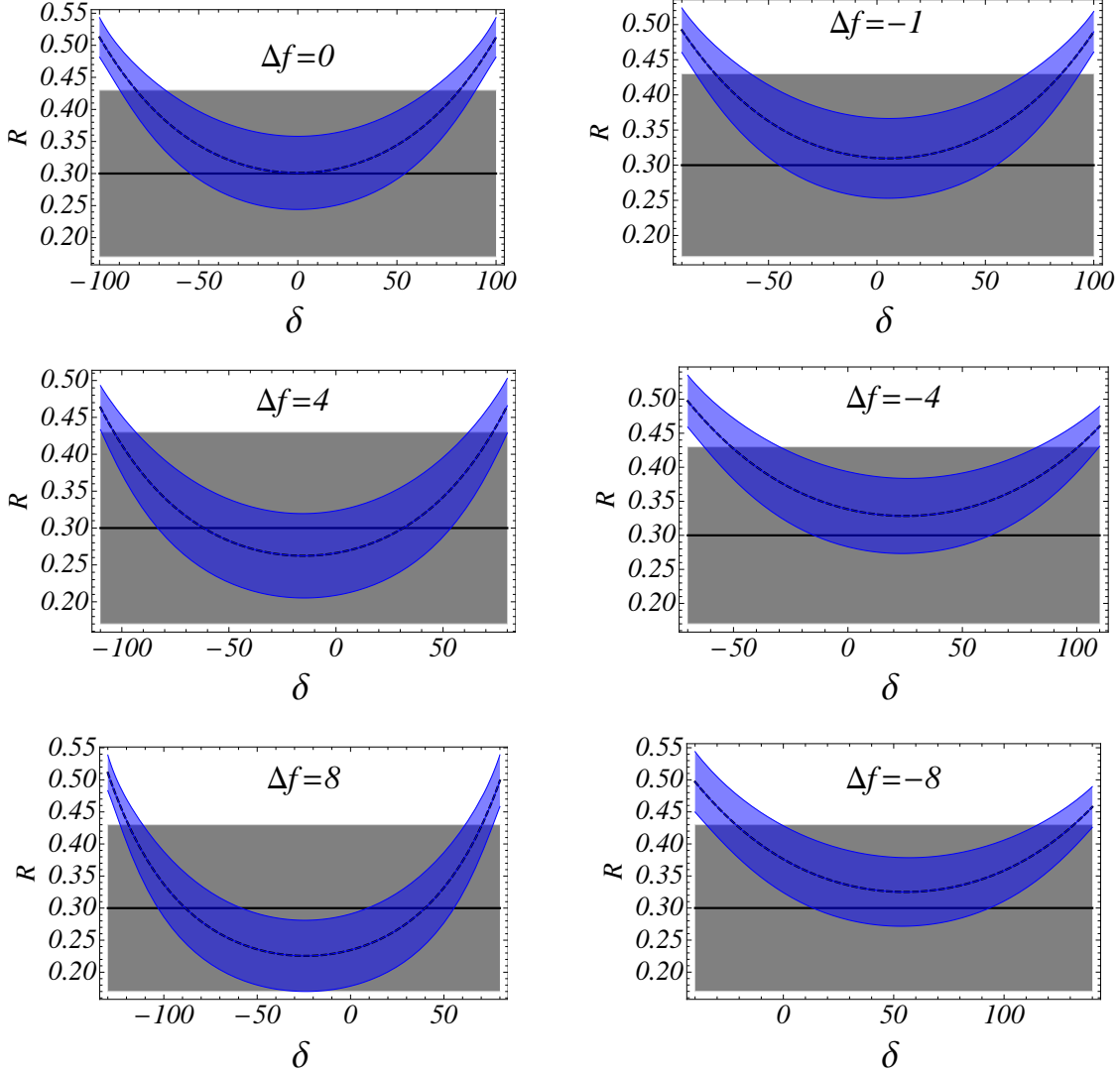


Figure 6: Ratio  $R_{\text{th}}$  (dashed) as a function of angle  $\delta$  (in degrees) for the different fixed values of parameter  $\Delta f$ . The experimental value  $R_{\text{exp}}$  is shown by solid line. The blue and gray shaded areas show theoretical and experimental uncertainties, respectively.

where  $\Delta f$  is unknown parameter. In the following we suppose that the colour-singlet soft-overlap contribution is smaller or of the same order as  $\Delta\mathcal{A}_s^{\perp(0)}$

$$|\Delta\mathcal{A}_s^{\perp(0)}(\Delta f)| \lesssim |\Delta\mathcal{A}_c^{\perp(0)}|, \quad (96)$$

that implies  $|\Delta f| \lesssim 10$ . In this case one obtains, for instance,

$$\Delta\mathcal{A}_s^{\perp(0)}(\Delta f = 4) = (-0.41 + 0.54i) \times 10^{-3}, \quad \Delta\mathcal{A}_{s\perp}^{\perp(0)}(\Delta f = 8) = (-0.81 + 1.1i) \times 10^{-3} \quad (97)$$

Numerical estimates of  $R_{\text{th}}$  in comparison with the  $R_{\text{exp}}$  are shown in Fig.6. The theoretical error band (blue shaded area) corresponds to variation of the DA parameters and value  $|\mathcal{A}_2^{\perp}|$  according to result in Eq(91). We see that for each value of  $\Delta f$  we have sufficiently large interval for the phase  $\delta$  which allows to describe the ratio  $R_{\text{exp}}$  within the error bars. The largest numerical effect from the symmetry breaking corrections is provided by the interference with large amplitude  $\mathcal{A}_2^{\perp}$ . From Fig.6 we conclude that reliable description of the data for the branching fractions can only be done taking into account both colour-octet and colour-singlet amplitudes.

In the previous sections it was shown that IR-singularities which appear in the convolution integrals of the colour-singlet amplitudes can be absorbed into the colour-octet amplitudes. Therefore one can define a regular colour-singlet contribution by subtraction of the IR-poles. Using such definition of the colour-singlet amplitudes one can try to estimate the value of colour-octet amplitude from the phenomenological value  $\mathcal{A}_2^\perp$  obtained in Eq.(91).

The colour-singlet amplitude is given by sum of the collinear  $\mathcal{A}_{2c}^{\perp(0)}$  and soft-overlap  $\mathcal{A}_{2s}^{\perp(0)}$  contributions given in Eqs.(21) and (55), respectively. The analytical expressions for the finite part of the collinear integrals are presented in Appendix B. Both amplitudes depends on the factorisation scales  $\mu$  or  $\nu$  which are set to  $m_c$ . Such scale setting removes the logarithms  $\ln m_c/\mu$  which must cancel in the sum of singlet and octet amplitudes. The values for parameters  $\Delta f$  and  $\delta$  are chosen according to results in Fig. 6. This allows us to obtain numerical estimates for the real and the imaginary parts of the colour-octet amplitude  $\mathcal{A}_2^{\perp(8)}$ . The obtained results are shown in Fig. 7. We see that the absolute value

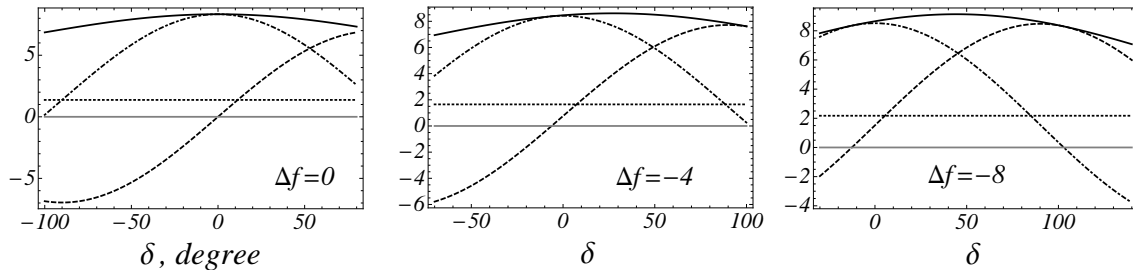


Figure 7: The colour-octet amplitude  $\mathcal{A}_2^{\perp(8)}$  in units  $10^{-3}$  as a functions of angle  $\delta$  at fixed  $\Delta f$ . The solid, dot-dashed and dashed lines correspond to absolute value, real and imaginary parts, respectively. The dotted line shows the absolute value of the colour-singlet amplitude  $|\mathcal{A}_2^{\perp(0)}|$ .

of the colour-octet amplitude is always few times larger than the colour-singlet one. But the values of the real and imaginary parts of the octet amplitude strongly depend on the phase  $\delta$ .

If the soft-overlap amplitude in Eq.(96) is underestimated then the value of the colour-singlet amplitude can be larger. But even if we take  $\Delta f = 20$  the colour-octet corrections remain sufficiently large and important. Therefore at least qualitatively we definitely can conclude that colour-octet mechanism plays very important role in the description of  $\chi_{Jc} \rightarrow \bar{K}K^*$  decays.

## 6 Discussion

Motivated by existing experimental data we discuss a description of decay amplitudes  $\chi_{cJ} \rightarrow \bar{K}K^*$  within the effective field theory framework. We find that the leading-order amplitude, which describes decay  $\chi_{c1} \rightarrow \bar{K}K_{\parallel}^*$ , is described by the colour-singlet operator but the corresponding contribution gives only about few percents of the measured branching ratio. We expect that the dominant effect is given by the subleading amplitudes which describe decays into transversely polarised vector meson  $\chi_{cJ\perp} \rightarrow \bar{K}K_{\perp}^*$ . The colour-singlet contributions for these amplitudes involve combinations of twist-2 and twist-3 collinear matrix elements as required by helicity conservation. In order to simplify our consideration we perform our calculations in the Wandzura-Wilczek approximation neglecting the twist-3 quark-gluon matrix elements. The computed colour-singlet amplitudes include the collinear convolution integrals which have infrared endpoint divergences. The structure of these singularities clearly indicates the mixing with a colour-octet operator. The corresponding colour-octet matrix element has been studied in the Coulomb limit using the pNRQCD framework. We obtain that UV-singularities of the octet contribution exactly reproduce the IR-singularities of the colour-singlet one and therefore these IR-divergencies can be absorbed into the renormalisation of the colour-octet matrix element. Hence a consistent description of the decay amplitudes  $\chi_{cJ\perp} \rightarrow \bar{K}K_{\perp}^*$  is only given by the sum of colour-singlet and colour-octet matrix elements. The effective field theory calculations also allow us to establish that the colour-octet amplitude has an imaginary part which is generated by the cut of the intermediate state with the bound heavy quark-antiquark in the octet configuration.

The heavy quark spin symmetry allows us to establish a relation between the colour-octet matrix elements for vector  $J = 1$  and tensor  $J = 2$  states. This makes it possible to do a computation of the spin symmetry breaking corrections which are free from the IR-divergencies. We compute these corrections using the physical subtraction scheme. We also include in our description a contribution of an unknown long distance matrix element describing soft-overlap configuration of the final mesons. Making various assumptions about the value of this matrix element we obtain a reliable description of the branching fractions. We conclude that the colour-octet contribution must be few times larger than the colour-singlet one.

The uncertainties in our consideration can be considerably reduced if one provides an estimate for the unknown soft-overlap matrix element. Potentially, the model independent information about this quantity can be obtained from the cross section of  $\gamma\gamma \rightarrow \bar{K}K^*$  process in the kinematical region where  $s \sim -t \sim -u \gg \Lambda_{QCD}^2$ . One can also compute the contributions with the twist-3 quark-gluon distribution amplitudes which have been discarded in this paper. We suppose that such contributions will improve the theoretical description but they will not change the qualitative conclusions of this work.

## Aknowlegements

I am grateful to M. Vanderhaeghen for attracting my attention to work [10] and for the discussions.

## 7 Appendix A. The long distance matrix elements

The NRQCD long distance matrix elements are defined as, see *e.g.* Ref. [4, 31]

$$\langle 0 | \frac{1}{2\sqrt{2}} \chi_\omega^\dagger \overleftrightarrow{D}_\mp^\alpha \left( \frac{-i}{2} \right) [\gamma_\mp^\alpha, \gamma_\mp^\beta] \gamma_5 \psi_\omega | \chi_{c1}(\omega) \rangle = \epsilon_X^\beta i \langle \mathcal{O}({}^3P_1) \rangle, \quad (98)$$

$$\langle 0 | \chi_\omega^\dagger \left( -\frac{i}{2} \right) \overleftrightarrow{D}_\mp^{(\alpha} \gamma_\mp^{\beta)} \psi_\omega | \chi_{c2}(\omega) \rangle = \epsilon_X^{\alpha\beta} i \langle \mathcal{O}({}^3P_2) \rangle, \quad (99)$$

The combination  $(\alpha, \beta)$  denotes the symmetrical traceless tensor. These operators are constructed from the quark  $\psi_\omega$  and antiquark  $\chi_\omega^\dagger$  four-component spinor fields satisfying  $\not{\omega}\psi_\omega = \psi_\omega$ ,  $\not{\omega}\chi_\omega = -\chi_\omega$ . The constants on the *rhs* of Eqs.(98) and (99) are related to the value of the charmonium wave functions at the origin. To leading order in small velocity  $v$  they read [31]

$$\langle \mathcal{O}({}^3P_J) \rangle \simeq \sqrt{2N_c} \sqrt{2M_{\chi_{cJ}}} \sqrt{\frac{3}{4\pi}} R'_{21}(0), \quad (100)$$

where  $R'_{21}(0)$  is the derivative of the quarkonium radial wave function. The value of this parameter has been estimated in the different potential models, see *e.g.* Ref. [36]. In this paper we use the value computed for the Buchmüller-Tye potential

$$m_c = 1.5 \text{ GeV}, \quad |R'_{21}(0)|^2 = 0.75 \text{ GeV}^5. \quad (101)$$

The leading twist  $K$  and  $K^*$  meson DAs has been studied in many publications, see *e.g.* [37–41] and references there in. The new updates of twist-2 and twist-3 DAs can be found in Refs. [42–44]. For a convenience of the reader, we briefly describe definitions and models which are used in this paper.

In the following we assume that direction  $z_\mu$  is light-like ( $z^2 = 0$ ) and  $[z, -z]$  denotes the appropriate Wilson line, see *e.g.* Ref. [42]. For pseudoscalar state  $\bar{K}(\bar{q}s)$  we need the following matrix elements

$$\langle \bar{K}(k) | \bar{s}(z)[z, -z] \gamma^\mu \gamma_5 q(-z) | \rangle = -i f_K k^\mu \int_0^1 dy e^{i(2y-1)(kz)} \phi_{2\bar{K}}(y), \quad (102)$$

$$\langle \bar{K}(k) | \bar{s}(z)[z, -z] i \gamma_5 q(-z) | \rangle = f_K \mu_K \int dy e^{i(2y-1)(kz)} \phi_{3\bar{K}}^p(y), \quad (103)$$

$$\langle \bar{K}(k) | \bar{s}(z)[z, -z] \sigma_{\mu\nu} \gamma_5 q(-z) | \rangle = \frac{i}{3} f_K \mu_K (k_\mu z_\nu - k_\nu z_\mu) \int_0^1 dy e^{i(2y-1)(kz)} \phi_{3\bar{K}}^\sigma(y). \quad (104)$$

Here

$$\mu_K = m_K^2 / (m_s + m_q), \quad (105)$$

and  $m_K, m_s, m_q$  denote the masses of the  $K$ -meson,  $s$ - and  $q = u, d$  quarks,  $f_K$  is the decay constant. The models for the corresponding DAs are given by the sum of the few first Gegenbauer moments ( $\bar{y} \equiv 1 - y$ )

$$\phi_{2\bar{K}}(y, \mu) = 6y\bar{y} \left( 1 + b_1(\mu)C_1^{3/2}(2y-1) + b_2(\mu)C_2^{3/2}(2y-1) \right), \quad (106)$$

$$\phi_{3\bar{K}}^p(x, \mu) = 1 + \rho_-^K \frac{3}{2}(1 + 6b_2(\mu)) \ln \frac{x}{\bar{x}} - \rho_-^K b_2(\mu) \frac{9}{2} \left\{ 6 C_1^{1/2}(2x-1) + C_3^{1/2}(2x-1) \right\}, \quad (107)$$

$$\phi_{3\bar{K}}^\sigma(x, \mu) = 6x\bar{x} \left\{ 1 - \rho_-^K b_2(\mu) \frac{15}{2} C_1^{3/2}(2x-1) \right\} + \rho_-^K (1 + 6b_2(\mu)) 9x\bar{x} \ln \frac{x}{\bar{x}}, \quad (108)$$

where  $\rho_\pm^K = (m_s^2 \pm m_q^2) / m_K^2$ , in Eqs.(107) and (108) we neglect numerically small terms  $\sim \rho_\pm^K b_1$ . Remind, that in this paper we do not consider the three-particle quark-gluons operators therefore such term are also neglected in expressions in Eqs.(107) and (108). The evolution of the various DA parameters are well known and explicit formulas can be found in the given references. In our numerical calculations we use the following values

$$m_{\bar{K}^0} = 498 \text{ MeV}, \quad m_s(2 \text{ GeV}) = 100 \text{ MeV}, \quad m_u \simeq m_d \approx 0. \quad (109)$$

$$f_K = 0.160 \text{ MeV}, \quad b_1(1 \text{ GeV}) = 0.06 \pm 0.03, \quad b_2(1 \text{ GeV}) = 0.30 \pm 0.15. \quad (110)$$

The required light-cone matrix elements for vector meson  $K^*(q\bar{s})$  read

$$\langle K^*(p, e^*) | \bar{q}(z)[z, -z] \sigma_{\mu\nu} s(-z) | 0 \rangle = -i f_{K^*}^\perp m_{K^*} (e_\mu^* p_\nu - e_\nu^* p_\mu) \int_0^1 dx e^{i(2x-1)(pz)} \phi_{2K^*}^\perp(x), \quad (111)$$

$$\langle K^*(p, e^*) | \bar{q}(z)[z, -z] \gamma_\sigma s(-z) | 0 \rangle = -i f_{K^*}^\parallel m_{K^*} \int_0^1 dx e^{i(2x-1)(pz)} \left\{ p_\sigma \frac{(e^* z)}{(pz)} \phi_{2K^*}^\parallel(x) + e_{\sigma\perp}^* \phi_{3K^*}^\perp(x) \right\}, \quad (112)$$

$$\langle K^*(p, e^*) | \bar{q}(z)[z, -z] \gamma_\sigma \gamma_5 s(-z) | 0 \rangle = f_{K^*}^\parallel m_{K^*} \frac{1}{2} i \varepsilon_{\sigma\rho\mu\nu} e^{*\rho} p^\mu z^\nu \int_0^1 dx e^{i(2x-1)(pz)} \psi_{3K^*}^\perp(x). \quad (113)$$

The corresponding models of DAs read

$$\phi_{2K^*}^{\parallel,\perp}(u) = 6u\bar{u} (1 + a_{1K^*}^{\parallel,\perp} C_1^{3/2}(2u-1) + a_{2K^*}^{\parallel,\perp} C_1^{3/2}(2u-1)), \quad (114)$$

$$\phi_{3K^*}^\perp(u) = \frac{1}{2} \int_0^u \frac{dv}{\bar{v}} \Omega(v) + \frac{1}{2} \int_u^1 \frac{dv}{v} \Omega(v) + \lambda_s^+ \phi_{2V}^\perp(u), \quad (115)$$

$$\psi_{3K^*}^\perp(u) = 2\bar{u} \int_0^u \frac{dv}{\bar{v}} \Omega(v) + 2u \int_u^1 \frac{dv}{v} \Omega(v), \quad (116)$$

with

$$\Omega(u) \simeq \phi_{2K^*}^\parallel(u) + \lambda_s^+ \frac{1}{2} (2u-1) \frac{d}{du} \phi_{2K^*}^\perp(u) + \lambda_s^- \frac{1}{2} \frac{d}{du} \phi_{2K^*}^\perp(u), \quad (117)$$

$$\lambda_s^- = \frac{f_{K^*}^\perp}{f_{K^*}^\parallel} \frac{m_s - m_q}{m_{K^*}}, \quad \lambda_s^+ = \frac{f_{K^*}^\perp}{f_{K^*}^\parallel} \frac{m_s + m_q}{m_{K^*}}. \quad (118)$$

For the DA parameters we use the numerical update from Ref. [44]

$$f_{K^*}^\parallel = 220 \text{ MeV}, \quad f_{K^*}^\perp(1 \text{ GeV}) = 185 \text{ MeV}, \quad m_{K^{*0}} = 896 \text{ MeV}, \quad (119)$$

$$a_{1K^*}^\parallel(1 \text{ GeV}) = -0.03 \pm 0.02, \quad a_{1K^*}^\perp(1 \text{ GeV}) = -0.04 \pm 0.03, \quad (120)$$

$$a_{2K^*}^\parallel(1 \text{ GeV}) = 0.11 \pm 0.09, \quad a_{2K^*}^\perp(1 \text{ GeV}) = 0.10 \pm 0.08. \quad (121)$$

Notice that we define  $SU(3)$  breaking coefficients  $a_{1K^*}^{\parallel,\perp}$  to be negative because  $K^*$  state includes  $s$ -antiquark.

## 8 Appendix B. Analytical results for the collinear convolution integrals

Here we provide results for the convolution integrals which describe colour-singlet amplitude  $A_{2c}^{\perp(0)}$ . These integrals have been computed using DAs described in the previous section. All the divergent integrals are computed using analytical regularisation prescription as described in the text. The singular terms (poles in  $1/\varepsilon$ ) are subtracted. The factorisation scales are fixed to be equal  $m_c$ . The resulting expressions have subscript “fin”. For simplicity we do not write explicitly the dependence on the factorisation scale in the parameters of DAs.

For the colour-singlet integrals in Eqs.(21) we obtain

$$\begin{aligned}
J_c^{(J=2)}[P_2 V_3]_{\text{fin}} = & \quad (122) \\
& \left\{ \Delta\phi'_{2P}(0)I[\bar{\Omega}] + \bar{\phi}'_{2P}(0)I[\Delta\Omega] \right\} \frac{1}{2} (1 - \ln 2) + \left\{ \bar{\phi}'_{2P}(0)\Delta\Omega(1) + \Delta\phi'_{2P}(0)\bar{\Omega}(1) \right\} \frac{1}{2} \left( 1 - \frac{\pi^2}{12} \right) \\
& + \frac{27}{16} b_1 \left\{ 8 + 3\pi^2 - 16 \ln 2 + a_2^{\parallel} (93 - 13\pi^2/4 - 16 \ln 2) \right\} \\
& - \frac{27}{16} b_1 \lambda_s^+ \left\{ 6\zeta(3) - 16 + 32 \ln 2 + \pi^2(4 \ln 2 - 6) + a_{2V}^{\perp} [36\zeta(3) - 516 + 352 \ln 2 + \pi^2(24 \ln 2 - 41)] \right\} \\
& + \frac{9}{16} a_{1V}^{\parallel} \left( 16 \ln 2 - 40 - \pi^2 + \frac{3}{2} b_2 \{ 260 - 49\pi^2 + 64 \ln 2 \} \right) \\
& + \frac{9}{16} \lambda_s^- \left( -32 \ln 2 + 4\pi^2 \ln 2 + 6\zeta(3) + 3b_2 \left\{ -64 \ln 2 + \pi^2(-15 + \frac{32}{3} \ln 2) + 12(10 + \zeta(3)) \right\} \right) \\
& + \frac{9}{16} \lambda_s^- a_{2V}^{\perp} \left\{ 36\zeta(3) + 400 + 2\pi^2(5 + 16 \ln 2) - 352 \ln 2 + 3b_2 [72\zeta(3) - 580 - 704 \ln 2 + \pi^2(155 + 48 \ln 2)] \right\} \\
& + \frac{27}{32} a_{1V}^{\perp} \lambda_s^+ \left\{ -12\zeta(3) - 80 + 96 \ln 2 - 2\pi^2(1 + 4 \ln 2) + b_2 [-72\zeta(3) + 60 + 576 \ln 2 - 3\pi^2(19 + 16 \ln 2)] \right\}. \\
\\
J_c^{(J=2)}[P_3 V_2]_{\text{fin}} = & \bar{\phi}_{2V}^{\perp}(0) \rho_-^K \left( -\frac{3}{2} \right) \left( 15b_2 + (1 + 6b_2) \frac{\pi^2}{12} - (1 + 21b_2) \ln 2 \right) + \Delta\phi_{2V}^{\perp}(1) (1 - \ln 2) \\
& - 9a_{1V}^{\perp} (2 \ln 2 - 4) - \frac{9}{2} \rho_-^K (\pi^2 + 4 \ln 2) (1 + 6a_{2V}^{\perp}) \\
& + \frac{27}{4} \rho_-^K b_2 (1 + 6a_{2V}^{\perp}) (20 + 3\pi^2 - 28 \ln 2). \quad (123)
\end{aligned}$$

The integrals for the vector state  $J = 1$  can be obtained using Eqs.(50) and (51).

## References

- [1] N. Brambilla *et al.* [Quarkonium Working Group Collaboration], hep-ph/0412158.
- [2] N. Brambilla *et al.*, Eur. Phys. J. C **71** (2011) 1534 doi:10.1140/epjc/s10052-010-1534-9 [arXiv:1010.5827 [hep-ph]].
- [3] G. T. Bodwin, E. Braaten and G. P. Lepage, Phys. Rev. D **46** (1992) R1914 doi:10.1103/PhysRevD.46.R1914 [hep-lat/9205006].
- [4] G. T. Bodwin, E. Braaten and G. P. Lepage, Phys. Rev. D **51** (1995) 1125 [Phys. Rev. D **55** (1997) 5853] [hep-ph/9407339].
- [5] J. Bolz, P. Kroll and G. A. Schuler, Phys. Lett. B **392** (1997) 198 doi:10.1016/S0370-2693(96)01515-8 [hep-ph/9610265].
- [6] J. Bolz, P. Kroll and G. A. Schuler, Eur. Phys. J. C **2** (1998) 705 doi:10.1007/s100520050174 [hep-ph/9704378].

- [7] S. M. H. Wong, Eur. Phys. J. C **14** (2000) 643 doi:10.1007/s100520000376 [hep-ph/9903236].
- [8] Y. Q. Chen and E. Braaten, Phys. Rev. Lett. **80** (1998) 5060 doi:10.1103/PhysRevLett.80.5060 [hep-ph/9801226].
- [9] M. Ablikim *et al.*, Phys. Rev. D **74** (2006) 072001 doi:10.1103/PhysRevD.74.072001 [hep-ex/0607023].
- [10] M. Ablikim *et al.* [BESIII Collaboration], Phys. Rev. D **96** (2017) no.11, 111102 doi:10.1103/PhysRevD.96.111102 [arXiv:1612.07398 [hep-ex]].
- [11] C. Patrignani *et al.* [Particle Data Group], Chin. Phys. C **40** (2016) no.10, 100001. doi:10.1088/1674-1137/40/10/100001
- [12] S. J. Brodsky and G. P. Lepage, Phys. Rev. D **24** (1981) 2848. doi:10.1103/PhysRevD.24.2848
- [13] V. L. Chernyak and A. R. Zhitnitsky, Nucl. Phys. B **201** (1982) 492 Erratum: [Nucl. Phys. B **214** (1983) 547]. doi:10.1016/0550-3213(82)90445-X, 10.1016/0550-3213(83)90251-1
- [14] V. L. Chernyak and A. R. Zhitnitsky, Phys. Rept. **112** (1984) 173. doi:10.1016/0370-1573(84)90126-1
- [15] X. H. Liu and Q. Zhao, Phys. Rev. D **81** (2010) 014017 doi:10.1103/PhysRevD.81.014017 [arXiv:0912.1508 [hep-ph]].
- [16] G. P. Lepage, L. Magnea, C. Nakhleh, U. Magnea and K. Hornbostel, Phys. Rev. D **46** (1992) 4052 [hep-lat/9205007].
- [17] A. Pineda and J. Soto, Nucl. Phys. Proc. Suppl. **64** (1998) 428 [hep-ph/9707481].
- [18] A. Pineda and J. Soto, Phys. Lett. B **420** (1998) 391 [hep-ph/9711292].
- [19] M. Beneke and V. A. Smirnov, Nucl. Phys. B **522** (1998) 321 [hep-ph/9711391].
- [20] N. Brambilla, A. Pineda, J. Soto and A. Vairo, Phys. Rev. D **60** (1999) 091502 [hep-ph/9903355].
- [21] N. Brambilla, A. Pineda, J. Soto and A. Vairo, Nucl. Phys. B **566** (2000) 275 [hep-ph/9907240].
- [22] N. Brambilla, A. Pineda, J. Soto and A. Vairo, Rev. Mod. Phys. **77** (2005) 1423 [hep-ph/0410047].
- [23] C. W. Bauer, S. Fleming and M. E. Luke, Phys. Rev. D **63**, 014006 (2000).
- [24] C. W. Bauer, S. Fleming, D. Pirjol and I. W. Stewart, Phys. Rev. D **63**, 114020 (2001).
- [25] C. W. Bauer and I. W. Stewart, Phys. Lett. B **516**, 134 (2001).
- [26] C. W. Bauer, D. Pirjol and I. W. Stewart, Phys. Rev. D **65**, 054022 (2002).
- [27] M. Beneke, A. P. Chapovsky, M. Diehl and T. Feldmann, Nucl. Phys. B **643**, 431 (2002).
- [28] M. Beneke and T. Feldmann, Phys. Lett. B **553**, 267 (2003).
- [29] M. Beneke and T. Feldmann, Nucl. Phys. B **592** (2001) 3 doi:10.1016/S0550-3213(00)00585-X [hep-ph/0008255].
- [30] M. Beneke, G. Buchalla, M. Neubert and C. T. Sachrajda, Nucl. Phys. B **606** (2001) 245 doi:10.1016/S0550-3213(01)00251-6 [hep-ph/0104110].
- [31] M. Beneke and L. Vernazza, Nucl. Phys. B **811** (2009) 155 doi:10.1016/j.nuclphysb.2008.11.025 [arXiv:0810.3575 [hep-ph]].
- [32] A. V. Manohar and I. W. Stewart, Phys. Rev. D **76** (2007) 074002 doi:10.1103/PhysRevD.76.074002 [hep-ph/0605001].
- [33] R. P. Feynman, "Photon-Hadron Interactions," Reading, 1972, 282p.



- [34] N. Isgur and C. H. Llewellyn Smith, Phys. Rev. Lett. **52**, 1080 (1984). N. Isgur and C. H. Llewellyn Smith, Nucl. Phys. B **317**, 526 (1989).
- [35] N. Kivel and M. Vanderhaeghen, JHEP **1602** (2016) 032 doi:10.1007/JHEP02(2016)032 [arXiv:1509.07375 [hep-ph]].
- [36] E. J. Eichten and C. Quigg, Phys. Rev. D **52** (1995) 1726 [hep-ph/9503356].
- [37] A. Khodjamirian, T. Mannel and M. Melcher, Phys. Rev. D **70** (2004) 094002 doi:10.1103/PhysRevD.70.094002 [hep-ph/0407226].
- [38] V. M. Braun and A. Lenz, Phys. Rev. D **70** (2004) 074020 doi:10.1103/PhysRevD.70.074020 [hep-ph/0407282].
- [39] P. Ball and R. Zwicky, Phys. Lett. B **633** (2006) 289 doi:10.1016/j.physletb.2005.11.068 [hep-ph/0510338].
- [40] V. M. Braun *et al.*, Phys. Rev. D **74** (2006) 074501 doi:10.1103/PhysRevD.74.074501 [hep-lat/0606012].
- [41] P. A. Boyle *et al.* [UKQCD Collaboration], Phys. Lett. B **641** (2006) 67 doi:10.1016/j.physletb.2006.07.033 [hep-lat/0607018].
- [42] P. Ball, V. M. Braun and A. Lenz, JHEP **0605** (2006) 004 doi:10.1088/1126-6708/2006/05/004 [hep-ph/0603063].
- [43] P. Ball and G. W. Jones, JHEP **0703** (2007) 069 doi:10.1088/1126-6708/2007/03/069 [hep-ph/0702100 [HEP-PH]].
- [44] P. Ball, V. M. Braun and A. Lenz, JHEP **0708** (2007) 090 doi:10.1088/1126-6708/2007/08/090 [arXiv:0707.1201 [hep-ph]].
- [45] J. Schwinger, J. Math. Phys. **5** (1964) 1606. doi:10.1063/1.1931195
- [46] M. Beneke, Y. Kiyo and K. Schuller, arXiv:1312.4791 [hep-ph].
- [47] M. Beneke, Y. Kiyo and A. A. Penin, Phys. Lett. B **653** (2007) 53 doi:10.1016/j.physletb.2007.06.068 [arXiv:0706.2733 [hep-ph]].
- [48] M. Beneke and Y. Kiyo, Phys. Lett. B **668** (2008) 143 doi:10.1016/j.physletb.2008.08.031 [arXiv:0804.4004 [hep-ph]].
- [49] N. Brambilla, M. A. Escobedo, J. Ghiglieri and A. Vairo, JHEP **1112** (2011) 116 doi:10.1007/JHEP12(2011)116 [arXiv:1109.5826 [hep-ph]].